https://doi.org/10.5194/egusphere-2025-4824
Preprint. Discussion started: 7 October 2025

Global Observations and European emissions of the halogenated olefins HFO-1234yf, HFO-1234ze(E), and HCFO-1233zd(E) from the AGAGE (Advanced Global Atmospheric Gases Experiment) network

Martin K. Vollmer[1], Joseph R. Pitt[2], Dickon Young[2], Stephan Henne[1], Blagoj Mitrevski[4], Jens Mühle[5], Anita Ganesan[3], Jgor Arduini[6,7], Alistair J. Manning[8,2], Thomas Wagenhäuser[9], Alison L. Redington[8], Brendan Murphy[2], Ray Gluckmann[10], Kieran M. Stanley[2], Paul B. Krummel[4], Chris R. Lunder[11], Jaegeun Yun[12], Dominique Rust[2], Angelina Wenger[2], Myriam Guillevic[13], Jooil Kim[5], Ray H. J. Wang[14], Tae Siek Rhee[15], Lionel Constantin[1], Arnoud Frumau[16], Christina M. Harth[5], Peter K. Salameh[17], Ove Hermansen[11], Andreas Engel[9], Simon O'Doherty[2], Sunyoung Park[12], Michela Maione[6,7], Paul J. Fraser[4], Ronald G. Prinn[18], Ray F. Weiss[5], and Stefan Reimann[1]

[1]Laboratory for Air Pollution / Environmental Technology, Empa, Swiss Federal Laboratories for Materials Science and Technology, Überlandstrasse 129, 8600 Dübendorf, Switzerland
[2]Atmospheric Chemistry Research Group, School of Chemistry, University of Bristol, Bristol, UK.
[3]School of Geographical Science, University of Bristol, Bristol, UK.
[4]CSIRO Environment, Aspendale, Victoria, Australia.
[5]Scripps Institution of Oceanography, University of California San Diego, La Jolla, California, USA.
[6]Department of Pure and Applied Sciences, University of Urbino, Urbino, Italy.
[7]Institute of Atmospheric Sciences and Climate, Italian National Research Council, Bologna, Italy.
[8]Met Office Hadley Centre, Exeter EX1 3PB, UK
[9]Institute for Atmospheric and Environmental Sciences, Goethe University, Frankfurt am Main, Germany
[10]Gluckman Consulting, Cobham, Surrey, KT11 2JH, UK
[11]NILU, Kjeller, Norway.
[12]School of Earth System Sciences, Kyungpook National University, South Korea.
[13]Federal Office for the Environment FOEN, Bern, Switzerland
[14]School of Earth and Atmospheric Sciences, Georgia Institute of Technology, Atlanta, Georgia, USA.
[15]Korea Polar Research Institute, KIOST, Incheon, South Korea.
[16]Department of Environmental Modelling, Sensing and Analysis, TNO, Netherlands Organisation for Applied Scientific Research, Petten, The Netherlands
[17]GC Soft Inc., Carlsbad, CA, USA
[18]Center for Global Change Science, Massachusetts Institute of Technology, Cambridge, Massachusetts, USA.

Correspondence: Martin K. Vollmer (martin.vollmer@empa.ch)

Abstract. Atmospheric observations of the widely used hydrofluoroolefins (HFOs) HFO-1234yf (2,3,3,3-tetrafluoroprop-1-ene), and HFO-1234ze(E) (E-1,3,3,3-tetrafluoroprop-1-ene), and the hydrochlorofluoroolefin (HCFO) HCFO-1233zd(E) (E-1-chloro-3,3,3-trifluoroprop-1-ene) are reported from the Advanced Global Atmospheric Gases Experiment (AGAGE) network. Since 2011, pollution events have grown in magnitude and frequency at sites which are influenced by regional emissions, while remote stations show first appearances of these substances. For HFO-1234yf and HFO-1234ze(E) winter peak mole fractions in background northern hemisphere air have grown from 0.03 ppt (picomol mol^{-1}, parts-per-trillion in dry air) in the

https://doi.org/10.5194/egusphere-2025-4824
Preprint. Discussion started: 7 October 2025

mid-2010s to 0.25 ppt in 2024, while the atmospherically more stable HCFO-1233zd(E) showed an increase from 0.06 ppt to 0.45 ppt. This suggests increasing usage of these haloolefins to replace hydrofluorocarbons (HFCs), which are regulated for phase-down over the next decades. Using European observations and the inverse modeling frameworks InTEM, ELRIS, and RHIME we determine emission trends and regional distribution. For Northwest Europe, emissions of HFO-1234yf increased steadily and rapidly from <0.1 Gg yr^{-1} in 2014 to 1.50 Gg yr^{-1} by 2023, presumably due to its introduction in the mobile air conditioning and refrigeration sectors. HFO-1234ze(E) emissions were low during 2014–2017, followed by a rapid increase in 2018/2019, potentially due its introduction as aerosol propellant, after which they increased more slowly to 0.96 Gg yr^{-1} by 2023. HCFO-1233zd(E) emissions are derived from 2017 onwards, showing a steady increase from 0.2 Gg yr^{-1} to 1.0 Gg yr^{-1} in 2023.

1 Introduction

Synthetically produced halocarbons have undergone several replacement and phase-out periods over the past decades. Their use in refrigeration, foam blowing, fire fighting, and solvent applications has led to emissions to the atmosphere, where they are involved in stratospheric ozone depletion and infrared radiation absorption, contributing to the enhanced greenhouse gas effect. The production and use of first generation halocarbons, e.g., chlorofluorocarbons (CFCs) and halons, have been largely phased out under the Montreal Protocol on Substances That Deplete the Ozone Layer since they deplete stratospheric ozone. Similarly, the transitional second generation hydrochlorofluorocarbons (HCFCs) have largely been phased out under the Montreal Protocol. The third generation products, hydrofluorocarbons (HFCs), do not destroy stratospheric ozone, but are strong greenhouse gases and hence were included in the Kigali Amendment to the Montreal Protocol in 2016 (United Nations, 2016) for a phase-down over the next decades. HFCs are currently being replaced by compounds with lower global warming potentials (GWP), including haloolefins. These are halogenated organic substances with an unsaturated carbon-carbon bond, resulting in much shorter atmosphere lifetime compared to saturated halocarbons (order of days to weeks, compared to years to decades). Hence, their GWP and their Ozone Depletion Potential (ODP) are small. Even though some environmental concerns exist, haloolefins are currently not included in the Montreal Protocol.

Haloolefins are included in the EU Regulation on fluorinated greenhouse gases 2024/573 (“2024 F-gas Regulation”, European Parliament and Council (2024)). Due to their low GWP, they are currently not included in the regulation’s phase-down from consumption, but they will be banned in various applications starting 2035 due to environmental concerns. In addition, emissions prevention and recovery regulations (Article 4), and recycling and destruction regulations (Article 8) will apply to haloolefins. Haloolefins are also within the scope of the definition of the very stable anthropogenic per- and polyfluoroalkyl substances (PFAS) for which there is currently an intense debate on regulations in the European Union. In January 2023, authorities from Denmark, Germany, the Netherlands, Norway, and Sweden submitted a REACH (Registration, Evaluation, Authorisation and Restriction of Chemicals) dossier for a restriction proposal for PFAS in the EU to the European Chemicals Agency (ECHA, European Chemicals Agency, 2024). It suggests a wide-ranging ban of PFAS from usage in many applications.

https://doi.org/10.5194/egusphere-2025-4824
Preprint. Discussion started: 7 October 2025

The predominant degradation pathway of this study's haloolefins from the atmosphere is initiated via reaction with the hydroxyl radical, while reaction with ozone and chlorine are negligible under environmental conditions (Nielsen et al., 2007; Søndergaard et al., 2007; Sulbaek Andersen et al., 2008, 2012; Madronich et al., 2023; Tewari et al., 2025). These compounds undergo complex atmospheric decay processes and there are concerns of harmful degradation products. In particular the formation of trifluoroacetic acid (TFA) is under active debate (Henne et al., 2012; Lindley et al., 2019; Behringer et al., 2021; David et al., 2021; Arp et al., 2024; Khan et al., 2025; Tewari et al., 2025; Henne et al., 2025; Hart et al., 2025). TFA is toxic and very stable under environmental conditions, raising concerns of accumulation in the environment. There is also an active debate on potential atmospheric degradation pathway to the potent greenhouse gas fluoroform (HFC-23) (Sulbaek Andersen and Nielsen, 2022; McGillen et al., 2023; Pérez-Peña et al., 2023; Thomson et al., 2025; Van Hoomissen et al., 2025). The synthesis of haloolefins is also complex with CFCs, HCFCs, and HFCs involved as precursors and intermediates (Sicard and Baker, 2020), leading to the debate of stricter control and emission reduction of these ODSs and potent greenhouse gases (Solomon et al., 2020).

The subjects of the present study are atmospheric observations and derived emissions of the most widely used hydrofluoroolefins (HFOs): HFO-1234yf (2,3,3,3-tetrafluoroprop-1-ene, $CF_3CF{=}CH_2$, CAS No. 754-12-1), and HFO-1234ze(E) (E-1,3,3,3-tetrafluoroprop-1-ene, *trans*-$CF_3CH{=}CHF$, CAS No 1645-83-6) and the hydrochlorofluoroolefin (HCFO) HCFO-1233zd(E) (E-1-chloro-3,3,3-trifluoroprop-1-ene, *trans*-$CF_3CH{=}CHCl$, CAS No. 102687-65-0). The three substances are mainly used in refrigeration, air conditioning, heat pumps (RACHP) and/or foam blowing. However, given the lack of reliable literature, it is difficult to evaluate the individual sectors in more detail, and also difficult to reconstruct the temporal changes in regulations and applications in various parts of the world.

Here, we provide information of usage patterns of the three haloolefins for the European Union (EU) and the UK, many of which may also apply to other parts of the world, although likely at different time frames. While this information remains anecdotal (without the ability to provide peer-reviewed literature citations) and estimates are based on bottom-up consumption models, which rely on assumptions regarding inventory and release functions, it is nevertheless helpful for the interpretation of our emission estimates.

HFO-1234yf is solely used in RACHP and for 2023 an estimated 77 % of it was used in pure form as the main replacement for HFC-134a in mobile air conditioning (MAC). The remaining 23 % was used in blends (mainly R448A and R449A), which are used in stationary refrigeration units. While these blends are drop-in replacements for older HFC-based refrigerants, they still contain significant amounts of HFCs with relatively high total GWPs (∼1400). They are therefore projected to be replaced in the near future by lower (<150) GWP refrigerants such as R454C and R455A (87 % and 84 % HFO-1234yf, respectively).

HFO-1234ze(E) is used in RACHP, foam blowing and as aerosol propellant but the individual shares of these three applications are poorly known to us. Usage in the RACHP sector is as pure fluid in medium-size chillers and in refrigeration blends (R448A and R450A) with GWPs of ∼600 as a replacement for HFC-134a. HFO-1234ze(E) is a foam blowing replacement compound for HFCs (mainly HFC-245fa and HFC-365mfc), which are banned for this application in the EU since 2023. The quantities used and their temporal evolution are not known to us, however, it is expected that this application contributes considerably to the emissions we derive for this compound. HFO-1234ze(E) is also used as an aerosol propellant as one of the

https://doi.org/10.5194/egusphere-2025-4824
Preprint. Discussion started: 7 October 2025

HFC-134a replacements in technical applications following the HFC-134a ban under the 2014 F-gas regulation (European Parliament and Council, 2014). A HFC-134a phase-down regulation is now also in place for metered dose inhalers (MDIs) for pharmaceutical use in the 2024 F-gas regulation (European Parliament and Council, 2024). HFO-1234ze(E) is currently tested as one potential replacement in this application. Overall, it is assumed that its application in aerosol sprays is contributing considerably to emissions in Europe, particularly as this application is fully emissive.

HCFO-1233zd(E) was originally marketed as a solvent but is now mainly used as foam blowing agent and in minor quantities in RACHP. The former is currently assumed to be the major emission source in the EU. With the ban of HCFC-123 in the EU in 2000, alternative refrigerants for large-scale low-pressure chillers were not available resulting in the use of different technologies. This situation changed recently when HCFO-1233zd(E) was identified as suitable for these chillers. While their applications (and resulting HCFO-1233zd(E) emissions) are currently assumed to be small, they will likely become more significant.

As these three substances are mainly replacing the HFCs in phase-down, it is expected that the transition to these chemicals will appear first in regions with accelerated phase-down schedules in the Montreal Protocol, and those with additional regulations, particularly in Europe (EU Regulation on fluorinated greenhouse gases 2024/573 (European Parliament and Council, 2024)), in the USA (American Innovation & Manufacturing (AIM) Act of 2020 (US-AIM, 2020)), Canada, and Australia.

Little is currently known about the atmospheric abundance and distribution of the three compounds. Their first atmospheric measurements were reported by Vollmer et al. (2015) from the semi-remote Jungfraujoch (Switzerland) station and from an urban site in Switzerland. Starting in 2014, the measurements of the three compounds were gradually extended to most stations of the Advanced Global Atmospheric Gases Experiment (AGAGE, https://tolnet.larc.nasa.gov/missions/agage/) network (Prinn et al., 2018; Western et al., 2025).

Here, we present HFO and HCFO observations from most AGAGE sites to the end of 2024 and we use the dense European station network in a detailed modeling study to estimate 10 years (2014–2023) of emissions from Northwest (NW) Europe. We compare these to emission estimates of the refrigerant HFC-134a derived from AGAGE measurements, to explore the transition from HFC-134a to the three haloolefins, in particular in the MAC sector (O'Doherty et al., 2004; Manning et al., 2021; Liang et al., 2022).

Because of the spatial sparsity of the observations in the AGAGE network we are currently unable to conduct other regional estimates. In addition, unlike the long-lived halocarbons, global or hemispheric emissions estimates using the AGAGE 12-box model (Cunnold et al., 1983; Rigby et al., 2013; Western et al., 2025) are not feasible due to their short atmospheric lifetimes.

2 Methods

2.1 Stations

In-situ measurements of the three haloolefins are currently conducted at most AGAGE stations (Fig. 1). In Europe, measurements are conducted at Zeppelin (Ny Ålesund, Spitsbergen), Mace Head (Ireland), Tacolneston (UK), Jungfraujoch (Switzerland), Monte Cimone (Italy, recent instrument upgrade) and most recently at Taunus (Germany, Meixner et al., 2025). They are

https://doi.org/10.5194/egusphere-2025-4824
Preprint. Discussion started: 7 October 2025

also measured at Trinidad Head (California, USA), Gosan (Jeju Island, South Korea), Ragged Point (Barbados), Cape Matatula (American Samoa), and Kennaook / Cape Grim (Tasmania, Australia), see Table 1. We also provide measurements of samples collected weekly at the South Korean Antarctic station King Sejong (South Shetland Islands) and analyzed at the Swiss Federal Laboratories for Materials Science and Technology (Empa), see Appendix C.

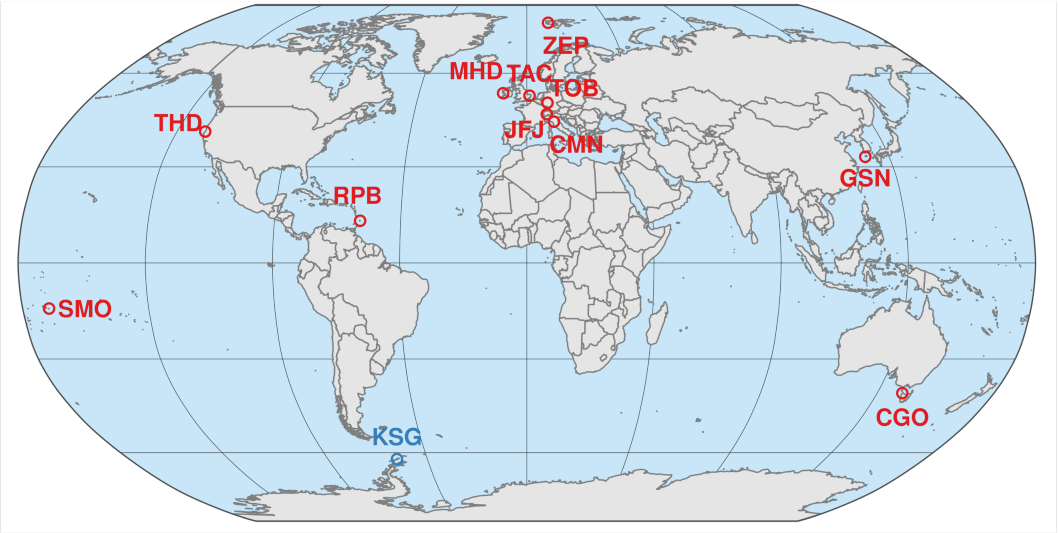

Figure 1. Location of the AGAGE (Advanced Global Atmospheric Gases Experiment) stations (in red) with publicly available measurements of HFO-1234yf ($CF_3CF=CH_2$), HFO-1234ze(E) (*trans*-$CF_3CH=CHF$), and HCFO-1233zd(E) (*trans*-$CF_3CH=CHCl$): Zeppelin, Spitsbergen (ZEP), Mace Head, Ireland (MHD), Tacolneston, UK (TAC), Taunus, Germany (TOB), Jungfraujoch, Switzerland (JFJ), Monte Cimone, Italy (CMN), Trinidad Head, California, USA (THD), Gosan, South Korea (GSN), Ragged Point, Barbados (RPB), Cape Matatula, American Samoa (SMO), and Kennaook / Cape Grim, Australia (CGO). Flask sample measurements are available from the South Korean Antarctic station King Sejong (in blue).

2.2 Analytical Setup

Measurements reported here are mostly based on Medusa gas chromatography mass spectrometry (GCMS) techniques (Miller et al., 2008; Arnold et al., 2012; Prinn et al., 2018). The Medusa-GCMS instruments at Monte Cimone and Taunus were recently built and installed (Tab. 1). These are the first commercially available Medusa-GCMS instruments (Markes International, UK), designed to closely follow the AGAGE custom built Medusa-GCMS instruments in functionality and operation. At Monte Cimone, haloolefins were already measured since 2017 using different instrumentation (Maione et al. (2013), and in overlap with Medusa-GCMS (Oct 2022 – Dec 2023).

On the Medusa-GCMS, typically a 2 L sample is pre-concentrated on a first cold trap filled with HayeSep D at ~ -160 °C before it is cryo-focused onto a second trap at similar temperature. In this process, remnants of oxygen and nitrogen and

https://doi.org/10.5194/egusphere-2025-4824
Preprint. Discussion started: 7 October 2025

Table 1. Station List and Data Availability for HFO-1234yf ($CF_3CF=CH_2$), HFO-1234ze(E) (*trans*-$CF_3CH=CHF$), and HCFO-1233zd(E) (*trans*-$CF_3CH=CHCl$).[a]

Station Name	Abbr	Network/ Institution	Lat °N	Lon °E	Altitude[b] (m.a.s.l.)	Instrument	Data availability [mm/yyyy] HFO-1234yf	HFO-1234ze(E)	HCFO-1233zd(E)
Zeppelin	ZEP	AGAGE	78.9	11.9	475	Medusa	03/2016 – 12/2024	11/2017 – 12/2024	01/2017 – 12/2024
Mace Head	MHD	AGAGE	53.3	-9.9	5	Medusa	02/2014 – 12/2024	02/2014 – 12/2024	02/2014 – 12/2024
Tacolneston	TAC	AGAGE	52.5	1.1	69	Medusa	09/2014 – 12/2024	02/2019 – 12/2024	02/2019 – 12/2024
Taunus	TOB	AGAGE	50.2	8.4	825	Medusa	02/2023 – 12/2024	02/2023 – 12/2024	02/2023 – 12/2024
Jungfraujoch	JFJ	AGAGE	46.5	8.0	3580	Medusa	01/2011 – 12/2024	09/2010 – 12/2024	02/2013 – 12/2024
Monte Cimone	CMN	AGAGE	44.2	10.7	2165	GCMS	09/2017 – 12/2023	09/2017 – 12/2023	03/2018 – 12/2023
Monte Cimone	CMN	AGAGE	44.2	10.7	2165	Medusa	10/2022 – 12/2024	10/2022 – 12/2024	10/2022 – 12/2024
Trinidad Head	THD	AGAGE	41.0	-124.1	107	Medusa	05/2017 – 12/2024	05/2017 – 12/2024	05/2017 – 12/2024
Gosan	GSN	AGAGE	33.3	126.2	72	Medusa	02/2016 – 12/2024	08/2018 – 12/2024	03/2019 – 12/2024
Ragged Point	RPB	AGAGE	13.2	-59.4	15	Medusa	08/2016 – 12/2024	01/2014 – 12/2024	04/2018 – 12/2024
Cape Matatula	SMO	AGAGE	-14.2	-170.6	42	Medusa	07/2018 – 12/2024	07/2018 – 12/2024	03/2018 – 12/2024
Kennaook/Cape Grim	CGO	AGAGE	-40.7	144.7	94	Medusa	11/2018 – 12/2024	11/2018 – 12/2024	11/2018 – 12/2024
King Sejong	KSG	KOPRI/Empa	-62.2	-58.8	2	Medusa flasks	01/2017 – 12/2024	01/2017 – 12/2024	01/2012 – 12/2024

a) Stations are listed in latitudinal order from north to south. Data availability for in situ and flask records with start and end dates.

Abbreviations are:
AGAGE: Advanced Global Atmospheric Gases Experiment.
KOPRI: Korea Polar Research Institute.
Empa: Swiss Federal Laboratories for Materials Science and Technology.
b) These are the altitudes of the science buildings. Air intake altitudes at most stations may be higher.

120 significant fractions of carbon dioxide and some noble gases are removed. The sample is then injected onto the chromatographic column (CP-PoraBOND Q, 0.32 mm ID × 25 m, 5 μm, Varian Chrompack) in the gas chromatograph (Agilent 6890 or 7890), purged with helium (grade 6.0), which is further purified using a getter (HP2, VICI, USA). The sample is detected in the quadrupole mass spectrometer in selected ion monitoring mode (initially Agilent model 5973s, later 5975/5977 models). For details on acquired fragment ions, mass spectra, retention times, and nonlinearity experiments, see Vollmer et al. (2015). On the
125 older Monte Cimone GCMS instrument (Tab. 1) with a Gaspro chromatographic column, HFO-1234yf and HFO-1234ze(E) are detected ∼10 s before HFC-134a and Halon-1211, respectively (using m/z 114 and 69) and HCFO-1233zd(E) is detected ∼8 s before HFC-245fa (using m/z 130 and 95). For most stations, the chromatograms for the measured fragments are remarkably clean from interferences by other compounds, and instrument blanks and memory effects are absent. Chromatographic peak integrations are set to reliably detect and integrate mole fractions larger than 0.01–0.02 ppt (parts-per-trillion, picomol mol^{-1})
130 for HFO-1234yf and HFO-1234ze(E) and 0.005–0.01 ppt for HCFO-1233zd(E), which we refer to as 'detectable levels' in the Results Section.

Repeated long-term measurements of the three haloolefins from whole-air calibration standards stored in 34 L internally electropolished stainless steel canisters (Essex Industries, Missouri, USA), as typically used in AGAGE, reveal stability over

https://doi.org/10.5194/egusphere-2025-4824
Preprint. Discussion started: 7 October 2025

years. These calibration standards are filled under 'wet' conditions (no active drying of the samples; water vapor is targeted near saturation pressure) to passivate the tanks' internal surfaces to avoid degradation of some measured compounds, foremost CCl_4. Whether this is necessary to maintain stability of the haloolefins is unknown to us. Also, we found that the haloolefins were preserved during passage through Nafion driers (Permapure, US) inside the Medusa-GCMS, in particular, no memory effects were observed (unlike some other compounds with carbon-carbon double bonds (e.g. propene)).

2.3 Calibration

The AGAGE calibration scheme is based on a hierarchy of whole-air standards compressed into "Essex" canisters. Secondary and tertiary standards are filled by the Scripps Institution of Oceanography (SIO) at La Jolla (California), while most quaternary/working standards (used to calibrate the individual instruments) are filled by station maintainers. All standards are generally filled under clean-air conditions using modified oil-less diving compressors (Rix Industries, USA) or cryogenic techniques. Since the abundances of these short-lived haloolefins are often very low or even absent in these air masses, which would result in a highly uncertain calibration scale propagation, the tanks are spiked with small quantities of haloolefins. This typically results in mole fractions of 0.5–1.5 ppt with chromatographic peak sizes well above detection limits. The three substances are the first (and currently only) species spiked into calibration tanks in a coordinated approach within the entire AGAGE network.

The primary calibration scales for these three substances were originally maintained by Empa (Vollmer et al., 2015). However, with the incorporation of these measurements into the AGAGE network, these scales were transferred to the AGAGE central calibration facility at SIO via the inter-comparison of a suite of calibration standards. This transfer allows for the maintenance of the calibration scales within a much larger selection of secondary reference standards at SIO and a more direct calibration of tertiary standards, which are exchanged with the field sites. These tertiary standards are used on site to propagate calibration onto the quaternary/working standards, which in turn are used to calibrate the instruments for air measurements.

For HFO-1234yf, the newly available METAS-2017 primary calibration scale (Guillevic et al., 2018) was adopted by AGAGE. It has an improved expanded uncertainty (1.5%, 2-sigma) compared to the Empa-2013 calibration scale (Vollmer et al., 2015). Based on a METAS-2017/Empa-2013 calibration scale conversion factor of 0.910, all older data were updated to the new primary calibration scale. The calibrations of HFO-1234ze(E) and HCFO-1233zd(E) remain on the Empa-2013 primary scales with assigned uncertainties of 15% (1-sigma) (Vollmer et al., 2015).

2.4 Calibration and Measurement Uncertainties

To derive accuracies for the reported measurements we follow an approach outlined in Vollmer et al. (2018) and combine three independent uncertainties: uncertainty of the calibration scales mentioned in the previous subsection, propagation uncertainty, and the instrumental precision of the measured air sample. The propagation uncertainty combines all uncertainties arising from the inter-comparisons of the standards used to propagate assigned mole fraction in the primary standards to the on-site quaternary (working) standards. We assume that the measurement uncertainties of these standards are the same for secondary, tertiary, and quaternary standards and treat them independently. The resulting propagation uncertainties (1σ) are $\sim 4\%$ for HFO-1234yf and HFO-1234ze(E), and $\sim 2\%$ for HCFO-1233zd(E). The uncertainties directly associated with the air sample

https://doi.org/10.5194/egusphere-2025-4824
Preprint. Discussion started: 7 October 2025

measurements on the Medusa-GCMS are highly mole-fraction dependent. For more polluted air masses with mole fractions greater than ∼ 1 ppt, the precisions are ∼ 2% for HFO-1234yf and HFO-1234ze(E), and ∼ 1% for HCFO-1233zd(E) as determined from repeated measurements of working standards of similar mole fractions. The resulting combined uncertainties for air samples with elevated mole fractions in polluted air are estimated at 7% for HFO-1234yf, and 16–20% for HFO-1234ze(E) and HCFO-1233zd(E), the latter two being dominated by the large calibration scale uncertainties. For direct comparisons of measurements reported within the AGAGE network including long-term atmospheric trends, the calibration scale uncertainties do not apply and the remaining uncertainties reduce to approximately 5–10% in more polluted air samples.

2.5 Inverse modeling

Three atmospheric inverse modeling systems were employed to estimate emissions of HFO-1234yf, HFO-1234ze(E) and HCFO-1233zd(E) from NW Europe (Belgium, Germany, France, UK, Ireland, Luxembourg and the Netherlands), using data from Mace Head, Tacolneston, Monte Cimone and Jungfraujoch (the Taunus observation records were deemed too brief). These systems are the Inverse Technique for Emission Modeling (InTEM, Arnold et al., 2018; Manning et al., 2021), the Regional Hierarchical Inverse Modeling Environment (RHIME, Ganesan et al., 2014), and Empa's Lagrangian Regional Inversion System (ELRIS, Henne et al., 2016; Katharopoulos et al., 2023). Each system utilizes output from an atmospheric transport model and a Bayesian optimization framework to estimate spatially-resolved emissions on a reduced resolution grid determined by the observation network. Total mole fractions are simulated as the sum of a regional fraction, determined by the emissions and the regional transport model, and a background contribution (boundary condition). The Bayesian approach minimizes the mismatch between the simulated and the observed atmospheric mole fractions, taking into account both the constraints imposed by the observation and model uncertainties and the uncertainties associated with a priori emissions.

All three systems have been applied in previous studies (e.g., Redington et al., 2023) and are only briefly described below, first in terms of their common aspects (transport model and prior emissions) and then individually for where they differ. In all cases observations were first averaged into 4-hour periods and individual inversions were performed independently for individual years, assuming constant emissions over the course of a year (no seasonality or trend considered). A posteriori emissions are presented without further temporal smoothing/aggregation (except the HFC-134a estimates taken from a previous study, which are presented with a 3-year rolling-average applied).

2.5.1 Transport model

All three systems utilized output from the Lagrangian particle dispersion model NAME (Numerical Atmospheric dispersion Modelling Environment, Jones et al. (2007)), which has been used in numerous inverse modeling studies (Arnold et al., 2018; Ganesan et al., 2020; Manning et al., 2021; Redington et al., 2023; Say et al., 2020). The NAME model is driven by 3-dimensional meteorological fields from the operational weather model operated by the UK Meteorological Office, the so-called Unified Model. The horizontal and vertical resolution of these fields varies over time with the development of the meteorological model (Manning et al., 2021, Table 1 therein). Over the present study period, the lowest meteorological resolution was ∼25 km in Jan 2014 increasing over time to a resolution of ∼12 km from July 2017 onward. The NAME model was run back-

https://doi.org/10.5194/egusphere-2025-4824
Preprint. Discussion started: 7 October 2025

wards in time to calculate source receptor relationships (SRRs), which provide the quantitative link between emission sources within the model domain and the measured mole fraction enhancement at the observation site. 20,000 particles per hour were released from each station and followed backwards in time for 30 days or until they leave the computational domain, which encompasses Europe, the Northern Atlantic and parts of North America. The release heights for Mace Head and Tacolneston were chosen to match the height of the inlet above ground level (10 m for Mace Head, 100 m for Tacolneston before February 2017 and 185 m afterwards). The release heights for the high-altitude stations were chosen to account for differences between the actual station elevation and the model orography at the station locations, with the latter being considerably lower due to smoothing at the given model resolution. Release heights of 1000 m and 500 m above ground level were found to be appropriate for Jungfraujoch and Monte Cimone, respectively.

Separate SRRs were stored for each hour of backward transport from release location. Because haloolefins have relatively short atmospheric lifetimes (compared for example to HFCs), they experience non-negligible atmospheric removal over the 30 day transport time of the NAME simulations. To account for this, an exponential decay of the SRRs was computed backward in time with hourly resolution and with an average, monthly atmospheric lifetime as described below. These lifetimes were assumed constant in space within the domain and constant in time within each month. The sum of these degraded hourly SRRs results in a single integrated 30-day SRR that accounts for atmospheric degradation for a specific HFO. The times and locations that particles left the computational domain were also recorded to provide the sensitivity to boundary conditions.

Representative atmospheric lifetimes for HFO-1234yf, which was released in Europe, were based on calculations by Henne et al. (2012) using the FLEXPART ("FLEXible PARTicle dispersion model") atmospheric transport model for simulations of European HFO-1234yf emissions. These simulations used prescribed atmospheric temperature (3-hourly resolution) and OH and Cl concentrations (monthly averages) to calculate explicit HFO-1234yf loss rates at each model particle. The total HFO-1234yf abundance divided by the total loss of HFO-1234yf in the simulation was then used to estimate monthly average lifetimes of HFO-1234yf, which were applied to NAME footprints.

For this project, the monthly mean lifetimes of HFO-1234ze(E) and HCFO-1233zd(E) were scaled to those explicitly calculated for HFO-1234yf using the average tropospheric (OH reactive loss) lifetimes (Burkholder and Hodnebrog, 2022) of 12 days for HFO-1234yf, 19 days for HFO-1234ze(E), and 42 days for HCFO-1233zd(E). The monthly mean lifetimes with minimum estimates for June and maximum estimates for December ranged form 3.6–42 days for HFO-1234yf, 5.7–66 days for HFO-1234ze(E), and 13–150 days for HCFO-1233zd(E) (Appendix D). The effects of including degradation is shown for the three compounds (Fig. D1) in Appendix D.

2.5.2 A priori Emissions

In the "base" case inversions, prior fluxes for all HFOs were distributed according to population density, scaled such that total annual emissions from NW Europe summed to 1 $\mathrm{Gg\,yr^{-1}}$ (arbitrarily chosen but representing 5–10 % of European HFO-1234yf emissions anticipated by Henne et al. (2012) for a complete replacement of HFC-134a by HFO-1234yf in mobile air conditioning). The observation of similarly large mole fraction peaks for HFO-1234ze(E) and HCFO-1223zd(E) as compared to HFO-1234yf at the European sites suggest that emissions of these compounds are at a similar order of magnitude. Hence,

https://doi.org/10.5194/egusphere-2025-4824
Preprint. Discussion started: 7 October 2025

as for HFO-1234yf, a priori emissions of 1 $\mathrm{Gg\,yr^{-1}}$ were assumed for NW Europe. A sensitivity test was also conducted using an alternative "flat" prior where 1 $\mathrm{Gg\,yr^{-1}}$ emissions over NW Europe were distributed uniformly over the land surface. Emissions outside NW Europe followed the same per-capita and per-surface-area emission factors as within NW Europe for the "base" and "flat" inversions, respectively. A priori uncertainties were chosen individually by each inversion system (see below).

2.5.3 Model-data-mismatch uncertainty

The three inversion systems use different methods to determine the model-data-mismatch uncertainty (or model-observation uncertainty). However, all three systems have in common that uncertainty contributions representing observational, representativeness, transport model, and background uncertainty are combined. The first two components are determined in the same way for all three inversion systems. The uncertainty of the observations is estimated to be 0.02 ppt or 10%, whichever is greater (representing measurement uncertainty only, excluding calibration scale and propagation uncertainties, see also subsection 2.4). The observed variability within individual 4-hr periods is used as a proxy for representativeness uncertainty. Transport model uncertainty itself is difficult and/or expensive to quantify objectively (Steiner et al., 2024). The three inversion systems followed slightly different approaches as outlined below.

2.5.4 InTEM

InTEM iteratively determines a grid with reduced spatial resolution as compared to the transport model. The grid design is driven by country borders, network sensitivity and iteratively updated emissions (Manning et al., 2021). Emissions on the reduced grid are solved for, assuming Gaussian a priori distributions and applying a non-negative solver to avoid negative fluxes. Uniform prior emissions over land were assumed for all three gases, with emissions of 1 $\mathrm{Gg\,yr^{-1}}$ and 40 % uncertainty over NWEU. InTEM simulates background mole fractions as a weighted average from the mole fractions encountered at 11 domain interfaces (Manning et al., 2021). The relative weight of each interface at a given time is based on the transport model simulation, providing information on where particles left the domain. Time-varying, site-specific a priori background mole fractions were derived from the observations at Mace Head, Jungfraujoch, and Monte Cimone as described by Manning et al. (2021). Tacolneston uses the same a priori background mole fraction as used at Mace Head. InTEM allows for a bias associated with each measurement site in the a posteriori solution. The a priori values for this bias were set to zero with a 1-sigma uncertainty of 0.0002 ppt.

The transport model uncertainty for each 4-hr period was taken as the larger of the median pollution (measured mole fraction enhancement above the modeled baseline) event in that year, or 10 % of the magnitude of the actual pollution event. Background uncertainty was assigned from the quadratic fit to the observations identified as baseline at the three stations as described in Manning et al. (2021).

A filter was applied to exclude observations measured under conditions where the NAME model is considered to perform less reliably. For surface sites, observations recorded when the surface boundary layer is lower than 200 m, or in strongly

https://doi.org/10.5194/egusphere-2025-4824
Preprint. Discussion started: 7 October 2025

stable atmospheres or when the local influence is very high are removed. For mountain stations, observations recorded when the boundary layer is with 100 m of the transport model release height (at JFJ, 1000 m and at CMN, 500 m) are removed.

2.5.5 RHIME

Groups of grid cells within the domain are aggregated into basis regions such that in each region the product of the average footprint (over all sites) and the prior emissions is above a threshold. This threshold is optimized to produce a target number of basis regions for the domain, which in this case was set to 250. A scaling factor of the a priori fluxes, sampled from a lognormal distribution with a mean of 1 and a standard deviation of 4, is then applied to each basis region. This distribution is only defined on the positive axis, thus preventing negative fluxes. In this case, this results in a prior uncertainty distribution for NW Europe with a 15.9 percentile of 0.69 $\mathrm{Gg\,yr^{-1}}$ and a 84.1 percentile of 1.27 $\mathrm{Gg\,yr^{-1}}$.

A priori boundary conditions were set to the monthly-mean mole fractions measured at MHD after filtering to only include data when the simulated wind direction was from the clean air sector (between 180° and 300°). Months with no data were forward filled from the previous month that did contain data. These a priori boundary conditions were then multiplied by a scaling factor sampled from a truncated normal distribution with a lower bound at zero (i.e., no negative mole fractions). The corresponding normal distribution (i.e., with the lower limit removed) would have a mean of 1 and a standard deviation of 0.5. The baseline mole fractions at a particular site for a given time were calculated as the weighted average of the boundary mole fractions, with the weights given by the fraction of model particles leaving the domain through each boundary.

Transport model uncertainty was calculated as a percentage of the measured mole fraction enhancement above the modeled baseline, where the percentage used for each year was optimized within the inversion. A minimum value (i.e., floor) for the combined model-data-mismatch uncertainty was also specified. This was calculated for each site by taking the monthly median measured mole fraction and subtracting the monthly 5th percentile measured mole fraction, then taking the annual mean of these monthly values. This minimum value was applied to account for the fact that transport error might result in modeled enhancements at the baseline points, even with an accurate flux map.

For the non-mountain sites (MHD and TAC), observations were filtered when the model boundary layer height was lower than 200 m above ground level and when the boundary layer height was less than 50 m above the inlet height. No filter was applied for the mountain sites (JFJ and CMN).

2.5.6 ELRIS

ELRIS optimized emissions on a reduced-resolution grid that exhibits finer resolution in areas of large average SRR (usually close to the observational sites) and coarser resolution in areas with low SRR. Areas below a certain threshold SRR and ocean-only grid cells were excluded from the optimization, but treated as part of four remote regions. In addition to emissions, background concentrations at the domain interfaces were optimized in ELRIS following the InTEM approach (Manning et al., 2021) with the difference of employing temporally variable mole fractions at the 11 domain interfaces that were varied monthly. A priori background mole fractions are constructed from a Robust Extraction of Baseline Signal (REBS) fit (Ruckstuhl et al., 2012) to the observations of the coastal site Mace Head that often represents the inflow into Europe. To avoid negative a

https://doi.org/10.5194/egusphere-2025-4824
Preprint. Discussion started: 7 October 2025

posteriori emissions ELRIS uses the approach suggested by Thacker (2007), which iteratively forces grid cells with negative a posteriori emissions to zero. A priori emission uncertainties were set such that uncertainties for each country in the inversion domain were 100 % of the emissions (1-σ level). Covariance between different a priori emissions were represented by an exponentially decaying influence with distance and a length scale of 500 km. The resulting total a priori uncertainty for NW Europe was approximately 50 %.

The transport model uncertainty is derived iteratively from the residuals of the simulated minus observed model fractions and contains a constant contribution and a contribution linearly growing with the simulated a priori mole fractions (Henne et al., 2016). It is scaled such that the a posteriori chi-square index (Berchet et al., 2013) becomes unity. The background uncertainty is set to that estimated by the REBS fit. Four iterations of the inversion are used to derive the final model-data-mismatch uncertainty.

For the non-mountain sites (MHD and TAC), observations were filtered using the same criteria as RHIME. For the mountain sites (JFJ and CMN) ELRIS applied a filter to exclude observations during times when the model boundary layer height was within 50 m of the particle release height.

3 Results and Discussion

3.1 Atmospheric Observations

Initially, the three haloolefins were only measured at Jungfraujoch (Vollmer et al., 2015), whereas measurements at most other stations began around 2015 (Figs. 2–5). However for many stations, the first few years of measurements were discarded because quaternary working and/or tertiary standards were not yet spiked with these species (see Methods), preventing accurately-calibrated air measurements. Fully calibrated measurements became available in 2014 from Mace Head and Ragged Point (for HFO-1234ze(E)) and starting in 2016–2018 from most other stations (Table 1). In general there is large variability in the observed mole fractions, depending on the proximity of the station to source regions and due to the short and seasonally varying lifetimes.

3.1.1 HFO-1234yf and HFO-1234ze(E)

At most sites, HFO-1234yf and HFO-1234ze(E) show a significant fraction of the observations below the detection limits in summer due to the much shorter lifetime during this season (Figs. 2, 4 and Appendix A Figs. A1 and Figs. A2). However, Northern Hemisphere (NH) sites with closer proximity to the pollution regions exhibit a large fraction of observations above detection limits. Large pollution events are recorded at the Tacolneston and Taunus stations, with HFO-1234yf frequently reaching 2–10 ppt (picomol mol^{-1}). Increased use of the HFOs in the NH is also reflected in the Mace Head record. There, mole fractions of the HFOs were often below the detection limit in all seasons during the early observational years (2014–2018). In recent years, winter-months mole fractions of HFO-1234yf and HFO-1234ze(E) were mostly above detection limit. Pollution events were very small and infrequent in 2014/2015, but have become more frequent and with larger magnitudes

https://doi.org/10.5194/egusphere-2025-4824
Preprint. Discussion started: 7 October 2025

(several ppt) after that. Also, these compounds are detected in air masses that have pronounced narrow footprints over the Atlantic and the American continent, and are likely to result from emissions in North America.

At the southern hemisphere sites Cape Matatula and Cape Grim / Kennaook, the majority of the measurements show undetectable HFOs. Nearly all detectable HFOs at Kennaook / Cape Grim are associated with air mass transport from the Melbourne region, $\sim$330 km north of the site. Even though the pollution events have become more frequent at these two sites, their magnitudes have never exceeded 1 ppt (HFO-1234yf) and 0.5 ppt (HFO-1234ze(E)).

Frequent pollution events are recorded at Gosan, suggesting that HFO-1234yf and HFO-1234ze(E) are also used within the footprint region of this station. Previous studies for other halocarbons (e.g. HFCs; Choi et al., 2024) measured at Gosan have shown large magnitudes of pollution, which strongly exceed those at other stations, e.g., Mace Head. This is different for the two HFOs (and also for HCFO-1233zd(E)) where we find pollution magnitudes at Gosan which are of similar size compared to Mace Head. These observations suggest a delayed replacement of HFC-134a by the HFOs in this SE Asian region compared to Europe. This is illustrated in Fig. 3a and Fig. 3b where we compare the pollution magnitudes of the two HFOs in relation to those for HFC-134a. We determine linear fits for the above-baseline pollution events of HFO-1234yf (ΔHFO-1234yf) against those of HFC-134a (ΔHFC-134a) for each year of observations using linear regression based on least-square methods (Fig. B1) and show these as timeseries in Fig. 3a and Fig. 3b. The linear fit slopes (ratios) increase strongly over the observational period, and are very similar for Jungfraujoch and Mace Head for each of the two HFOs. However, the increase of the ratio at Gosan is much smaller over the same time. This is indicative of a faster transition from HFC-134a to HFO-1234yf and HFO-1234ze(E) for Europe compared to the footprint regions of Gosan, in line with the stringent HFC phase-out regulations in Europe.

https://doi.org/10.5194/egusphere-2025-4824
Preprint. Discussion started: 7 October 2025

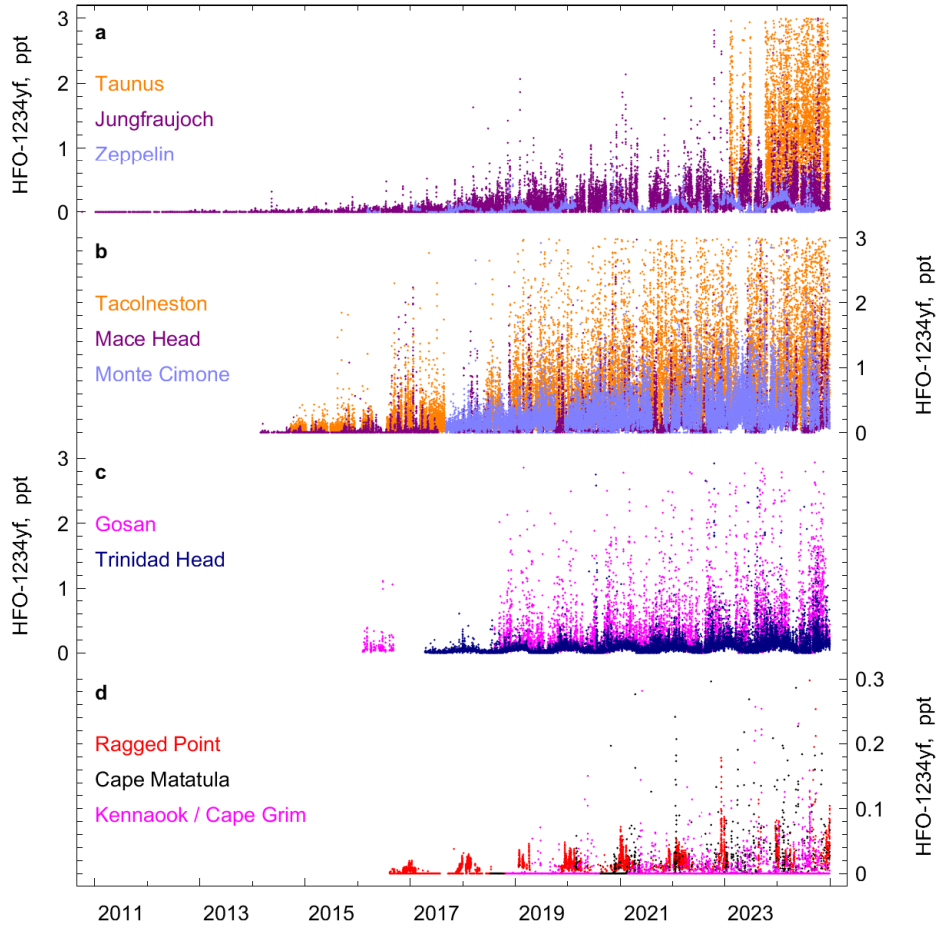

Figure 2. In situ observations of HFO-1234yf ($CF_3CF{=}CH_2$) from AGAGE stations. The records are separated into four subpanels for better visualization. a) Taunus (Germany), Jungfraujoch (Switzerland), Zeppelin (Spitsbergen). b) Tacolneston (UK), Mace Head (Ireland), Monte Cimone (Italy). c) Gosan (Jeju Island, South Korea), Trinidad Head (California, USA). d) Ragged Point (Barbados), Cape Matatula (American Samoa), and Kennaook / Cape Grim (Tasmania, Australia). Mole fractions larger than 3 ppt (0.3 ppt for panel d) are omitted from the plot.

https://doi.org/10.5194/egusphere-2025-4824
Preprint. Discussion started: 7 October 2025

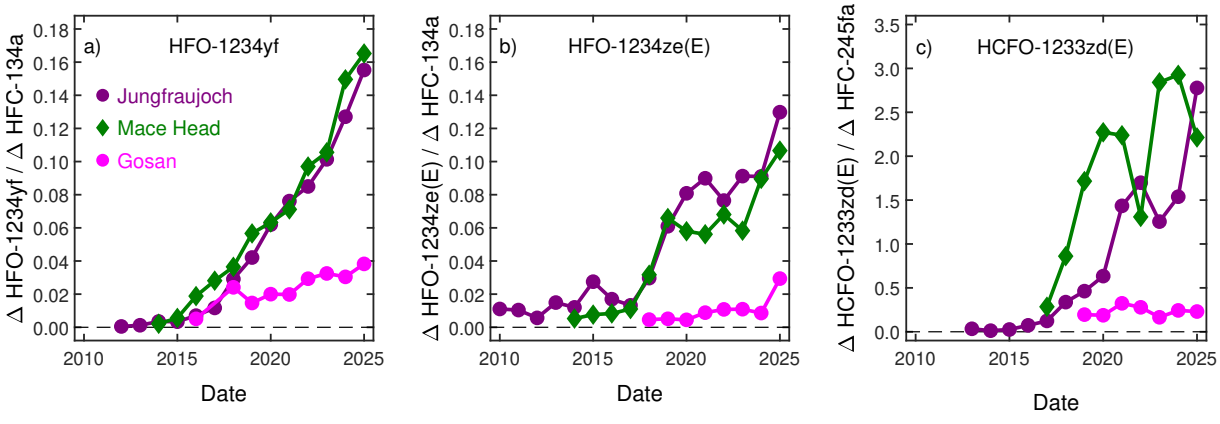

Figure 3. Ratios of pollution magnitudes (above baseline, Δ) of HFO-1234yf (a) and HFO-1234ze(E) (b) to HFC-134a and of HCFO-1233zd(E) to HFC-245fa (c) at Jungfraujoch, Mace Head, and Gosan. Assuming co-located sources and ignoring decay of the substances during transport, the elevated ratios found at Jungfraujoch and Mace Head compared to Gosan suggest an earlier replacement of HFC-134a and HFC-245fa by the HFOs and HCFO-1233zd(E), respectively, in Europe compared to the source region covered by Gosan.

https://doi.org/10.5194/egusphere-2025-4824
Preprint. Discussion started: 7 October 2025

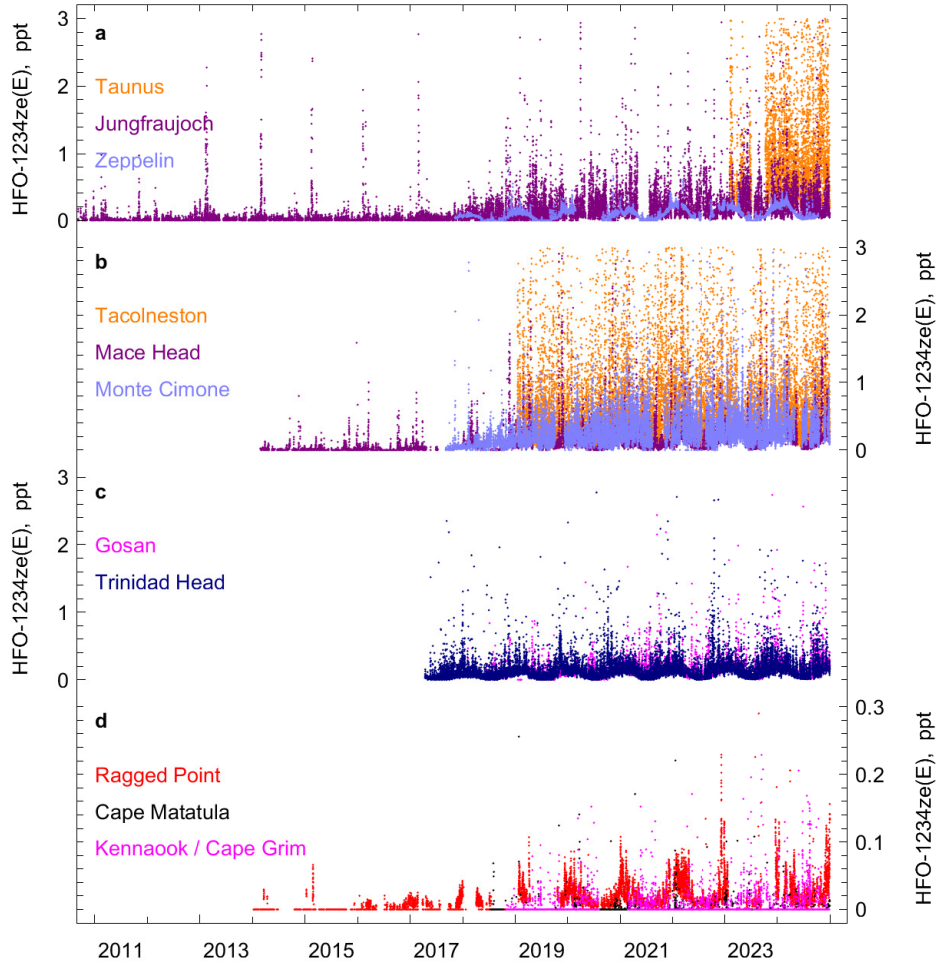

Figure 4. In situ observations of HFO-1234ze(E) (*trans*-$CF_3CH{=}CHF$) from AGAGE stations. The records are separated into four sub-panels for better visualization. a) Taunus (Germany), Jungfraujoch (Switzerland), Zeppelin (Spitsbergen). b) Tacolneston (UK), Mace Head (Ireland), Monte Cimone (Italy). c) Gosan (Jeju Island, South Korea), Trinidad Head (California, USA). d) Ragged Point (Barbados), Cape Matatula (American Samoa), and Kennaook / Cape Grim (Tasmania, Australia). Mole fractions larger than 3 ppt (0.3 ppt for panel d) are omitted from the plot.

https://doi.org/10.5194/egusphere-2025-4824
Preprint. Discussion started: 7 October 2025

3.1.2 HCFO-1233zd(E)

For HCFO-1233zd(E) more measurements are at detectable mole fraction levels compared to the two HFOs (Fig. 5). While for the earlier records, this was mainly due to lower analytical detection limits, in more recent years this is attributed to the longer lifetime (roughly doubled compared to the two HFOs). Early Jungfraujoch observations showed HCFO-1233zd(E) mole fractions that were about one order of magnitude smaller compared to the HFOs, and much fewer pollution events in the footprints of the station. Since 2016 almost all observations of HCFO-1233zd(E) in NH air masses reveal detectable mole fractions. The only exception is the tropical remote Ragged Point station where some NH air masses contained undetectable HCFO-1233zd(E) up to 2018 but not in more recent years. HCFO-1233zd(E) at Gosan is also above detection limits except for short periods with pronounced SH advection. In general, the seasonal apex (maximum) background HCFO-1233zd(E) mole fractions have exceeded those of the HFOs in the NH. The combination of fewer emissions and longer lifetime leads to a much more pronounced seasonality in the measurement records, and fewer pollution episodes, most clearly seen at Zeppelin. There the apex of the background mole fractions has increased from 0.07 ppt in early 2017 to 0.4 ppt at the end of 2023. Only the two SH sites at Samoa and Cape Grim exhibit a significant fraction of undetectable HCFO-1233zd(E) in their records. However, during the austral summer 2021/2022 all measurement at the two sites contained detectable HCFO-1233zd(E). First clear detection of HCFO-1233zd(E) at Antarctic King Sejong started in austral winter 2021 (Appendix C).

At Gosan, HCFO-1233zd(E) pollution events are similar in magnitude to Mace Head. To illustrate the delayed replacement of HFCs by HFCO-1233zd(E) we proceed in analogy to the two HFOs but because foam blowing is the main application for HCFO-1233zd(E), we here compare to HFC-245fa (Fig. 3c). Like for the two HFOs, the pollution ratios at Gosan compared to Mace Head and Jungfraujoch, (ΔHCFO-1233zd(E)/ΔHFC-245fa) suggest a delayed replacement of HFC-245fa by HCFO-1233zd(E) in the footprint region of Gosan (Fig. 3c, Fig. B2).

3.2 Northwest European (NW) Emissions

Observation-based emissions for the three haloolefins are determined using the three model frameworks: InTEM, ELRIS and RHIME. These 10-year emission timeseries (7-year for HCFO-1233zd(E)) are shown in Fig. 6 for the individual frameworks and for their multi-model mean. InTEM emission estimates for HFC-134a are also shown; these are taken from the model runs used in the 2025 UK National Inventory Document (NID) submitted to the United Nations Framework Convention on Climate Change (UNFCCC) (https://unfccc.int/). Given that European measurements of the haloolefins started already at the time of the market phase-in of these chemicals, we are able to derive their entire emission histories. Consequently, the emissions of HFO-1234yf (Fig 6b) and HFO-1234ze(E) (Fig 6c) are virtually absent at the beginning of the investigated period in 2014. Here, we only present results from our base inversions (lifetime-aware source sensitivities, population-based a priori distribution). Additional sensitivity tests (assuming inert tracer and uniform/flat a priori) are given in Appendices D and E1.

For HFO-1234yf, NW European emissions increased from 0.03 Gg yr^{-1} in 2014 to 1.50 Gg yr^{-1} in 2023. This increase is likely dominated by its phase-in in MAC, in replacement of HFC-134a. Over the same time period, HFC-134a emissions have not increased, supporting this interpretation. The relatively linear increase in HFO-1234yf emissions suggest that the transition

https://doi.org/10.5194/egusphere-2025-4824
Preprint. Discussion started: 7 October 2025

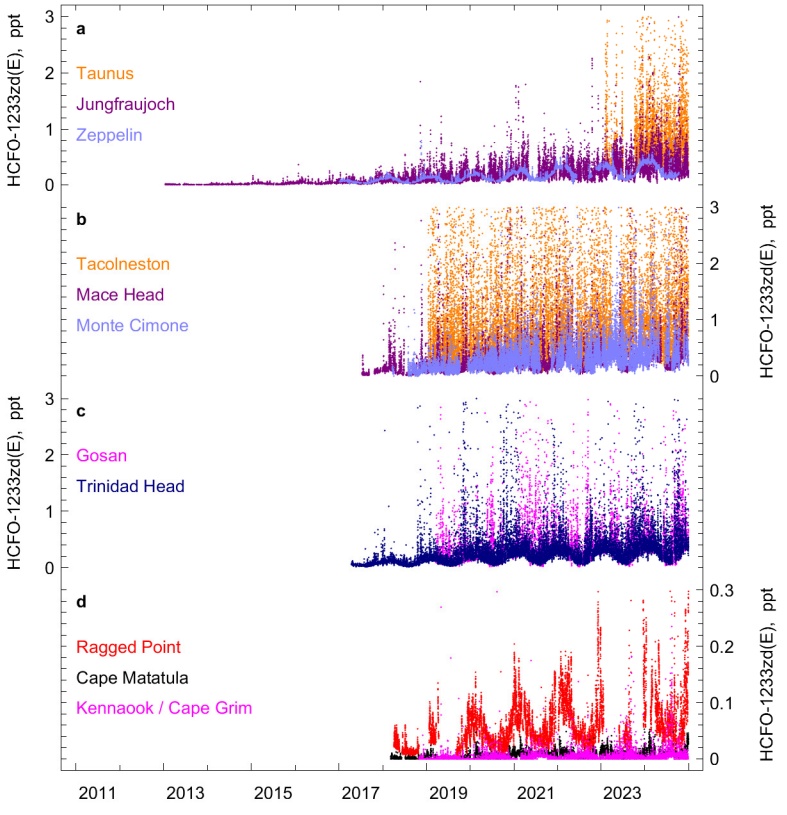

Figure 5. In situ observations of HCFO-1233zd(E) (*trans*-$CF_3CH{=}CHCl$) from AGAGE stations. The records are separated into four sub-panels for better visualization. a) Taunus (Germany), Jungfraujoch (Switzerland), Zeppelin (Spitsbergen). b) Tacolneston (UK), Mace Head (Ireland), Monte Cimone (Italy). c) Gosan (Jeju Island, South Korea), Trinidad Head (California, USA). d) Ragged Point (Barbados), Cape Matatula (American Samoa), and Kennaook / Cape Grim (Tasmania, Australia). Mole fractions larger than 3 ppt (0.3 ppt for panel d) are omitted from the plot.

https://doi.org/10.5194/egusphere-2025-4824
Preprint. Discussion started: 7 October 2025

in MAC was gradual. This is in line with a gradual phase-in of HFO-1234yf into the European vehicle fleet as the EU MAC regulation (European Parliament and Council, 2006), which came into effect in January 2017, applies only to new vehicles.

Using a population-based extrapolation from the NW Europe countries (254 million people in 2023, EUROSTAT, 2025b) to the EU27+ (27 EU countries plus the UK, Switzerland, and Norway, 530 million people in 2023), results in 3.1 Gg for 2023 for EU27+. Alternatively, almost identical emissions (3.2 Gg) are obtained if we upscale emissions based on number of passenger cars (in 2023, NW Europe 139 million vs 296 million in the EU27+, EUROSTAT, 2025a).

In contrast to the linear increase of the HFO-1234yf emissions, that of HFO-1234ze(E) (Fig 6c) shows two inflection points. Emissions initially stayed relatively low (2014–2017), followed by a rapid increase, before slowing down again and reaching 0.96 Gg yr^{-1} in 2023 (population-based extrapolation to EU27+ results in 2.00 Gg yr^{-1}). This pattern is robust against selective onsets of some measurement sites as was tested by dropping selective sites. It is also seen in the four largest emission regions (France, Germany, UK, and Benelux, see Appendix F). The reasons for this rapid onset are unclear. One could be the EU ban on the use of HFC-134a in technical aerosols, starting in January 2018. This could have boosted the use of HFO-1234ze(E), even though other alternatives (HFC-152a, hydrocarbons and dimethylether) also became available. Since this application results in immediate and complete emissions, such a replacement could explain the derived rapid emission increase. If the increase of ∼0.7 Gg HFO-1234ze(E) over the 2018–2019 resulted in a corresponding decrease of HFC-134a emissions, it would be difficult to detect within the overall large HFC-134a emissions. Another potential regulation causing the rapid growth in HFO-1234ze(E) emissions is the EU 2020 ban on HFCs in foam, which may have been met with an early change to HFO-1234ze(E). 2018 is also the start of the Kigali Amendment HFC phase-down which may have caused a strong increase in the use of HFO-1234ze(E).

HCFO-1233zd(E) emissions (derived from 2017 onward) increased steadily (similar to HFO-1234yf), reaching 1.04 Gg in 2023. A population-based extrapolation to EU27+ results in 2.17 Gg in 2023.

In Fig. 7 we show the geographical distributions of the changes in emission strength for NW Europe for 2014–2018 and 2019–2023. For HFC-134a the emission distribution is comparably invariant over the two periods while emission centers for HFO-1234yf and HFO-1234ze(E) appear only in the second period. For HFO-1234yf, the geographical distribution of the emissions for 2019–2023 resembles that for HFC-134a strongly and suggests that the use of HFO-1234yf is in similar applications as that for HFC-134a (most likely MAC). HFO-1234ze(E) also shows a similar distribution for 2019-2023, but for HCFO-1233zd(E) emissions centers are strongly biased towards the UK and Benelux countries and appear already in the 2017–2018 period. This suggests that the introduction of this chemical occurred differently in individual European countries. Reasons for this may be regulatory (HCFO-1233zd(E) contains a chlorine and permissions for use may be handled differently) or that its use in specific applications (e.g., foam blowing) was delayed in some countries.

https://doi.org/10.5194/egusphere-2025-4824
Preprint. Discussion started: 7 October 2025

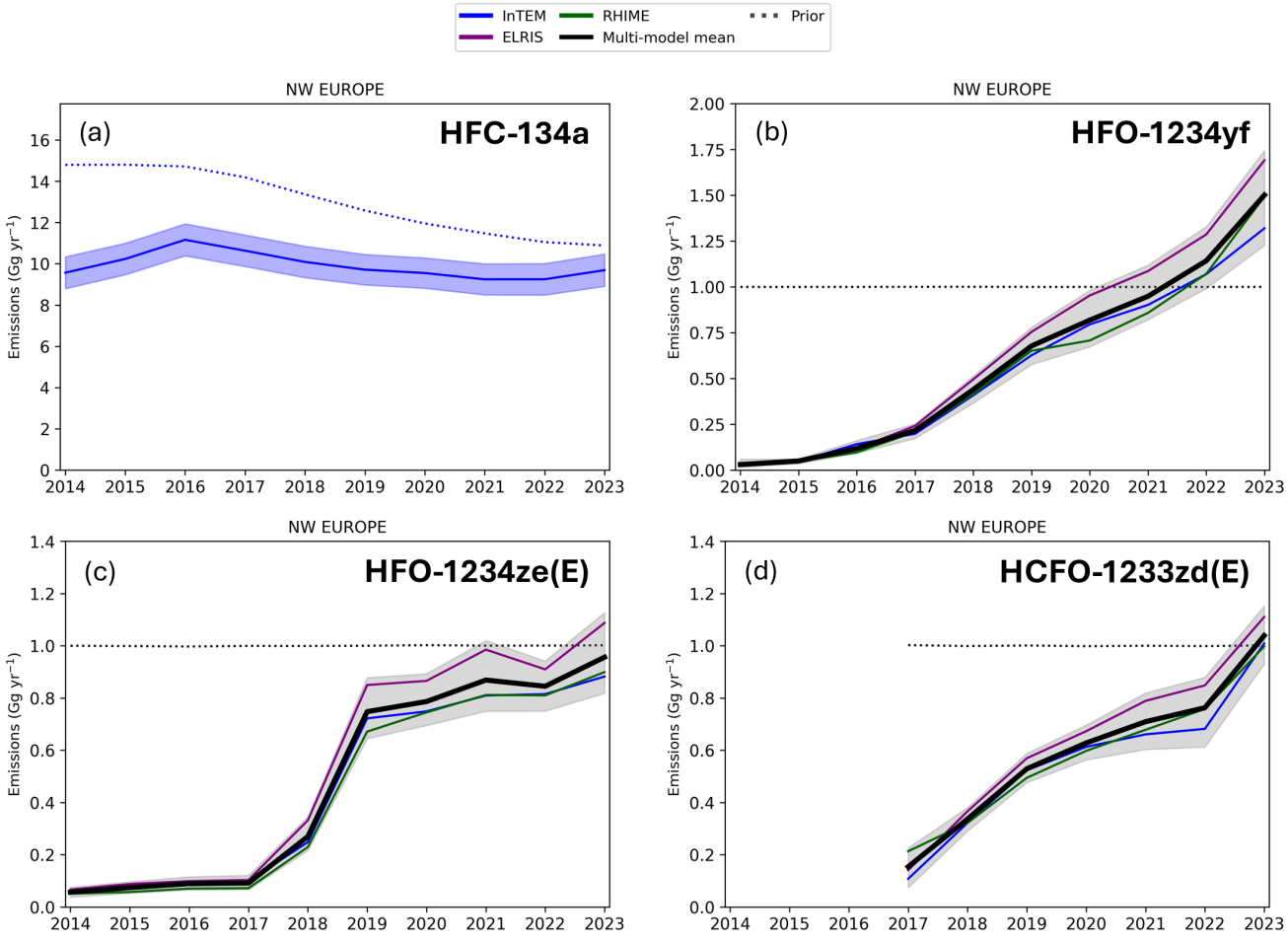

Figure 6. Emissions of HFC-134a, HFO-1234yf, HFO-1234ze(E), and HCFO-1233zd(E) from Northwest (NW) Europe (Belgium, Germany, France, UK, Ireland, Luxembourg and the Netherlands). Emissions are shown for the three model approaches InTEM, ELRIS, and RHIME and for their multi-model mean. The uncertainty range shown in grey is bounded by the 15.9 percentile of the lowest model and the 84.1 percentile of the highest model. Prior emissions for the three haloolefins are set uniformly at 1 Gg yr^{-1}. Emissions are increasing monotonically and strongly for the haloolefins during the observational periods. For HFO-1234ze(E), the large increase in the emissions in 2018 and 2019 is a robust feature and also seen in the countries with the largest emissions (France, Germany, and UK, see Appendix F). Emissions of HFC-134a are from InTEM only, 3-year smoothed and are taken from the model runs used in the 2025 UK NID submitted to the UNFCCC (with a range representing the 1σ posterior uncertainty).

https://doi.org/10.5194/egusphere-2025-4824
Preprint. Discussion started: 7 October 2025

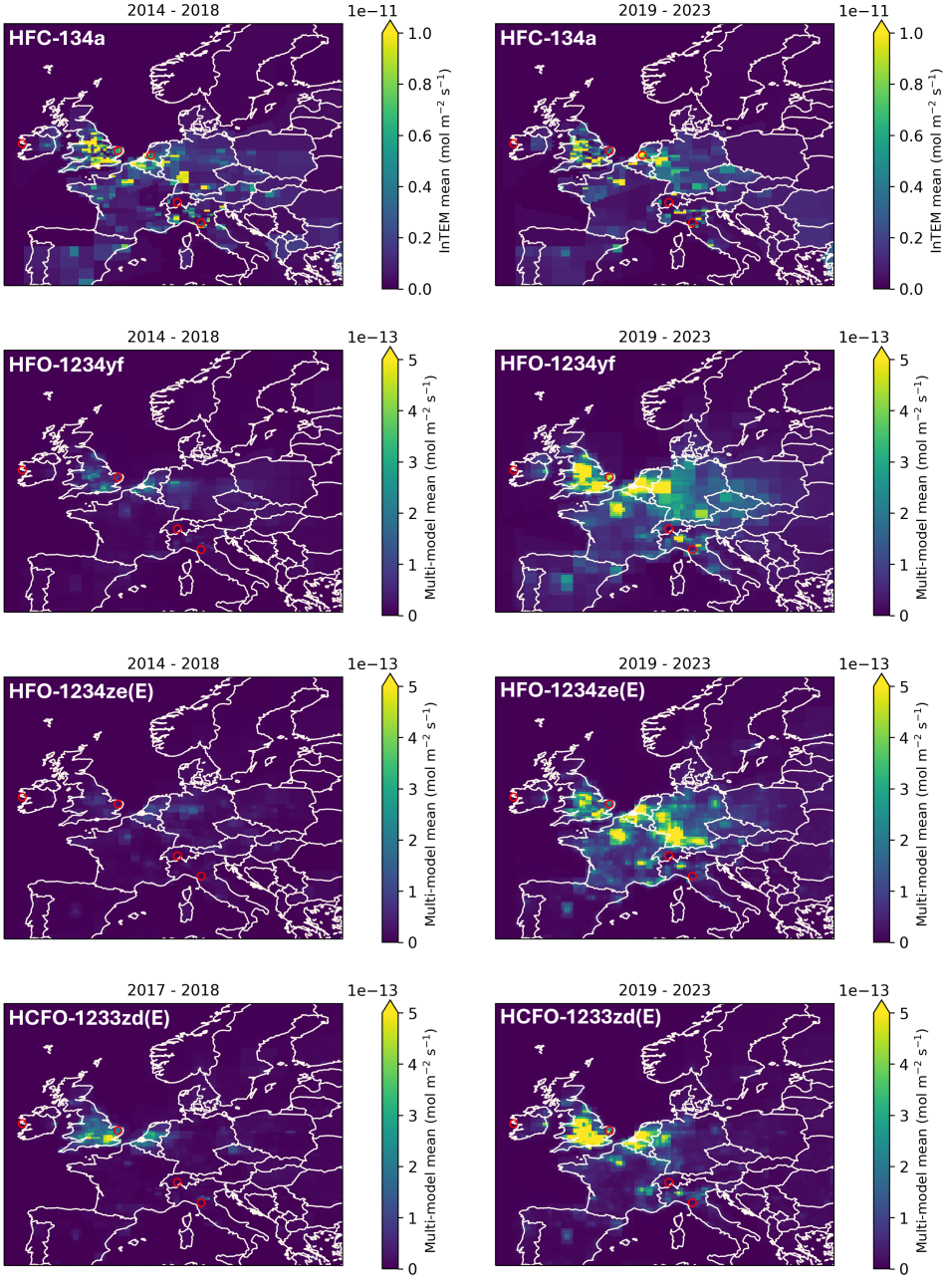

Figure 7. Emissive flux maps for Northwest (NW) European for HFC-134a, HFO-1234yf, HFO-1234ze(E) and HCFO-1233zd(E) for 2014–2018 (2017–2018 for HCFO-1233zd(E)) in the left panels and for 2019–2023 in the right panels. The scale for HFC-134a is two orders of magnitude larger than those for the haloolefins. Red circles denote measurement sites and are, from west to east, Mace Head (Ireland), Tacolneston (UK), Cabauw (NL, for HFC-134a from flask samples only), Jungfraujoch (Switzerland), and Monte Cimone (Italy).

https://doi.org/10.5194/egusphere-2025-4824
Preprint. Discussion started: 7 October 2025

4 Conclusions

We report on the first large-scale AGAGE network observations of HFO-1234yf, HFO-1234ze(E), and HCFO-1233zd(E), three recently marketed haloolefins used as replacements for HFCs. We estimate emissions for specific regions and countries in NW Europe and find increasing emissions to 1.50 Gg, 0.96 Gg, and 1.0 Gg by 2023, for HFO-1234yf, HFO-1234ze(E), and HCFO-1233zd(E), respectively. We conclude this as evidence of an ongoing transition away from HFCs, which are phased-down under the F-gas regulation and the Kigali Amendment of the Montreal Protocol. Support for this conclusion comes from stagnant emissions of HFC-134a (Manning et al., 2021), which is one of the main HFCs targeted for phase down. Our results allow for comparison with inventory emissions as soon as these will be publicly available. Because of the spatial sparsity of the observations in the AGAGE network we are currently unable to conduct regional estimates other than for Northwest Europe. Emission estimates on a global level using box models (e.g. AGAGE 12-box model Cunnold et al., 1983; Rigby et al., 2013; Western et al., 2025) are inappropriate given their coarseness and the short atmospheric lifetimes of the haloolefins. However, more sophistical global models such as GEOS-Chem (e.g. Bey et al., 2001; Tewari et al., 2025; GEOS-Chem, 2023) or STOCHEM (e.g. Holland et al., 2021), that include detailed chemistry could potentially be applied to gain a more complete picture of overall global emissions. This could be complemented by further regional studies of Asian regions, which should become possible as more measurements become available from there. The present data base can also support studies of atmospheric decay products e.g., TFA deposition, which are necessary to assess the environmental impact of the haloolefins. Since the atmospheric chemistry and environmental effects of the haloolefins are still poorly understood, it is crucial to further our understanding on the atmospheric abundances and emissions of these substances.

https://doi.org/10.5194/egusphere-2025-4824
Preprint. Discussion started: 7 October 2025

Code and data availability. Observations: High-resolution measurements from the AGAGE stations are available from https://www-air.larc.nasa.gov/missions/agage/. Comment to the editor and the reviewers: The high-resolution AGAGE observations will not be made publicly available until potential acceptance for publication of the manuscript. However, all data can be made available to the editor and the reviewers during the review process if needed.

Measurements of the three substances are also available from other sites (mostly urban or insufficiently long records), which are not covered in this paper. In-situ measurements are available on request from the co-authors of the respective institutions: at Dubendorf, Beromünster, Sottens (all Switzerland) and Cabauw (The Netherlands) from Empa, at La Jolla (California) from SIO, at Ridge Hill (UK, University of Bristol). Flask measurements are available from samples collected at Cabauw (The Netherlands), Hanimaadhoo (Republic of Maldives), and Bhola Island (Bangladesh) from the University of Bristol.

Inverse modeling code and data availability: Code availability: The code for RHIME can be obtained from github: https://github.com/openghg/openghg_inversions. The full model output is available on request. The numeric results for the emissions estimates are provided as a supplement.

https://doi.org/10.5194/egusphere-2025-4824
Preprint. Discussion started: 7 October 2025

Acknowledgements. We acknowledge the station personnel at all stations for their continuous support in conducting in situ measurements. AGAGE operations are supported by the National Aeronautics and Space Administration (NASA) Upper Atmosphere Research Program with grants 80NSSC21K1369 to MIT and grants 80NSSC21K1210 and 80NSSC21K1201 to SIO and multiple preceding grants for the lab operations at SIO and the support of Trinidad Head and Cape Matatula, and partial support of Ragged Point, Mace Head, and Kennaook / Cape Grim. We acknowledge the National Oceanic and Atmospheric Administration (NOAA) for operating the Cape Matatula observatory. Mace Head and Tacolneston, as part of the UK DECC Network, are also supported through the UK Government's Department for Energy Security and Net Zero under contract nos. TRN1028/06/2015, TRN1537/06/2018, TRN5488/11/2021 and prj_1604 to the University of Bristol. Further support for Barbados is provided by NOAA, contracts RA-133-R15-CN-0008, 1305M319CNRMJ0028 and 1305M324P0411 to the University of Bristol. Kennaook / Cape Grim is supported by the Commonwealth Scientific and Industrial Research Organization (CSIRO Australia), the Bureau of Meteorology (Australia), the Department of Climate Change, Energy, the Environment and Water (Australia), Refrigerant Reclaim Australia, the Australian Refrigeration Council,and through the NASA award to MIT with subaward to CSIRO for Cape Grim (80NSSC21K1369). Support for the measurements at the other stations is provided; for Jungfraujoch by the Swiss National Programs HALCLIM and CLIMGAS-CH (Swiss Federal Office for the Environment, FOEN) and by the International Foundation High Altitude Research Stations Jungfraujoch and Gornergrat (HFSJG); for Zeppelin by the Norwegian Environment Agency; for Monte Cimone by the Italian component of ACTRIS (Aerosol, Clouds and Trace Gases Research Infrastructure), under the Programma Operativo Nazionale Ricerca e Innovazione 2014–2020 PIR01 00015 "PER-ACTRIS-IT"; for Taunus the Medusa instrument was funded as part of the German ACTRIS programme and the operation was partly funded by the PARIS (Process Attribution of Regional Emissions) EU Project (Grant Agreement 10108430); for Gosan by the National Research Foundation of Korea (NRF) grant funded by the Ministry of Science and ICT (No. RS-2023-00229318). The King Sejong flask sample programme is partially supported by the Korea Polar Research Institute's Antarctic Monitoring Program (PE25170), several preceding grants (PE13410 and PE20150) and earlier also by the Swiss State Secretariat for Education and Research and Innovation (SERI). Funding for the Cabauw flask sampling and analysis for HFC-134a in the present study was provided to TNO by the Dutch Ministry of Economic Affairs and Climate Policy and the Ruisdael Observatory as part of the Dutch research program National Roadmap Large-scale Research Infrastructure with project number 184.034.015. The regional inverse modeling was supported by a model development programme organized through the PARIS project. The RHIME model runs were carried out using the computational facilities of the Advanced Computing Research Centre, University of Bristol (http://www.bristol.ac.uk/acrc/). Model data post-processing and plotting utilized the python package fluxy (Ramsden et al., 2025). FLEXPART simulations were carried out at the Swiss National Supercomputing Centre (CSCS) under institutional contract ID em05.

Author contributions. Sampling, Measurements and/or analytical work are performed by mkv, jp, dy, bm, jm, ja, tw, kms, crl, jy, dr, aw, mg, jk, af, cmh, oh, ae, so, pbk, tsr, data processing and quality control by mkv, jp, dy, bm, jm, ja, tw, kms, crl, jy, dr, aw, mg, jk, lc, cmh, oh, ae, so, pbk, sp, mm, sr, pjf, rgp, rfw, pks; inventory details by rg; modeling work by jp, sh, ag, alr, am, bm, rhjw instrument software by pks, dy, article written by mkv with contributions from most co-authors.

Competing interests. the authors declare no competing interest.

https://doi.org/10.5194/egusphere-2025-4824
Preprint. Discussion started: 7 October 2025

Appendix A: Detection limits

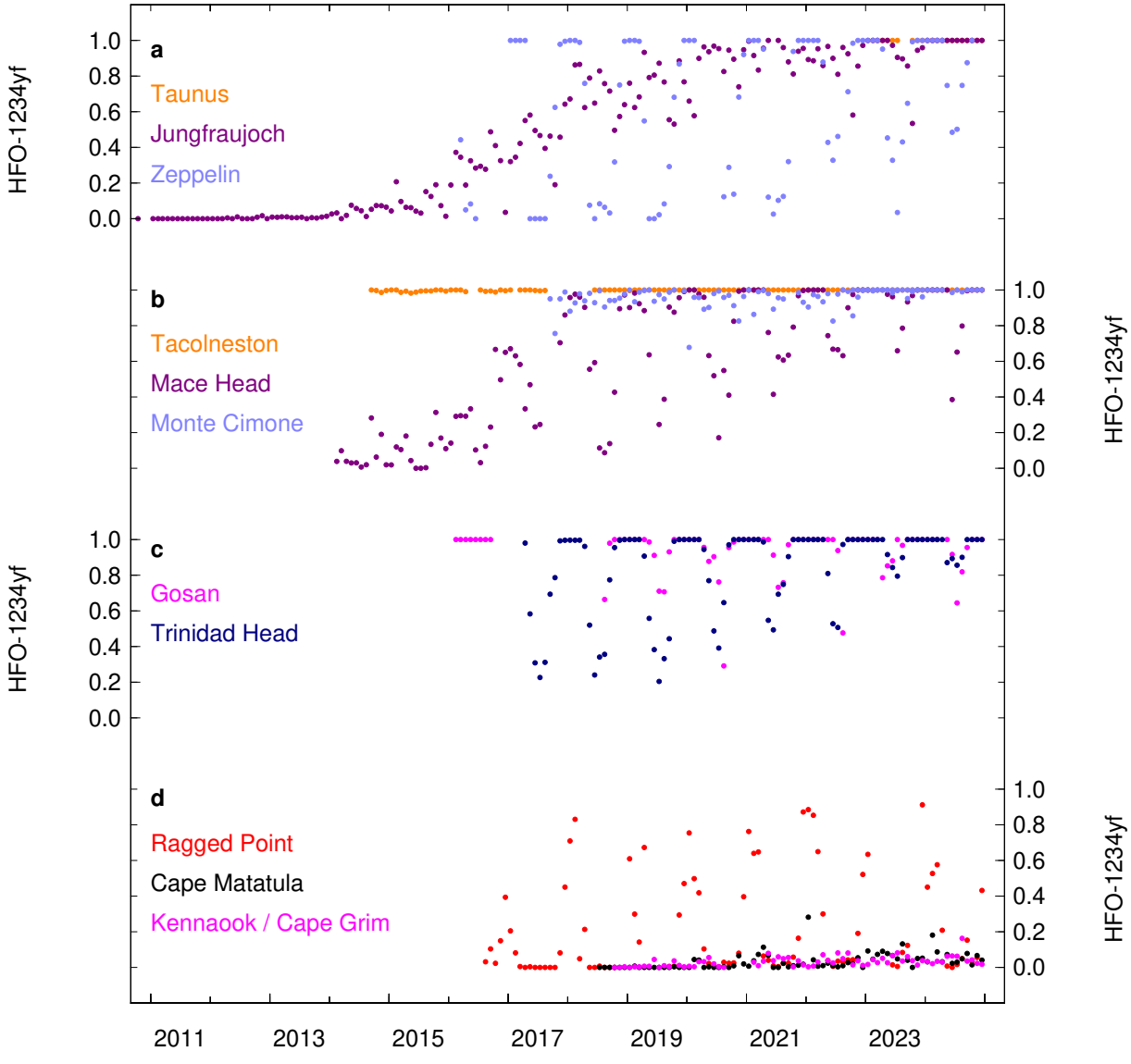

Figure A1. Ratio of the number of detectable to total measurements (monthly bins) for HFO-1234yf from AGAGE stations.

https://doi.org/10.5194/egusphere-2025-4824
Preprint. Discussion started: 7 October 2025

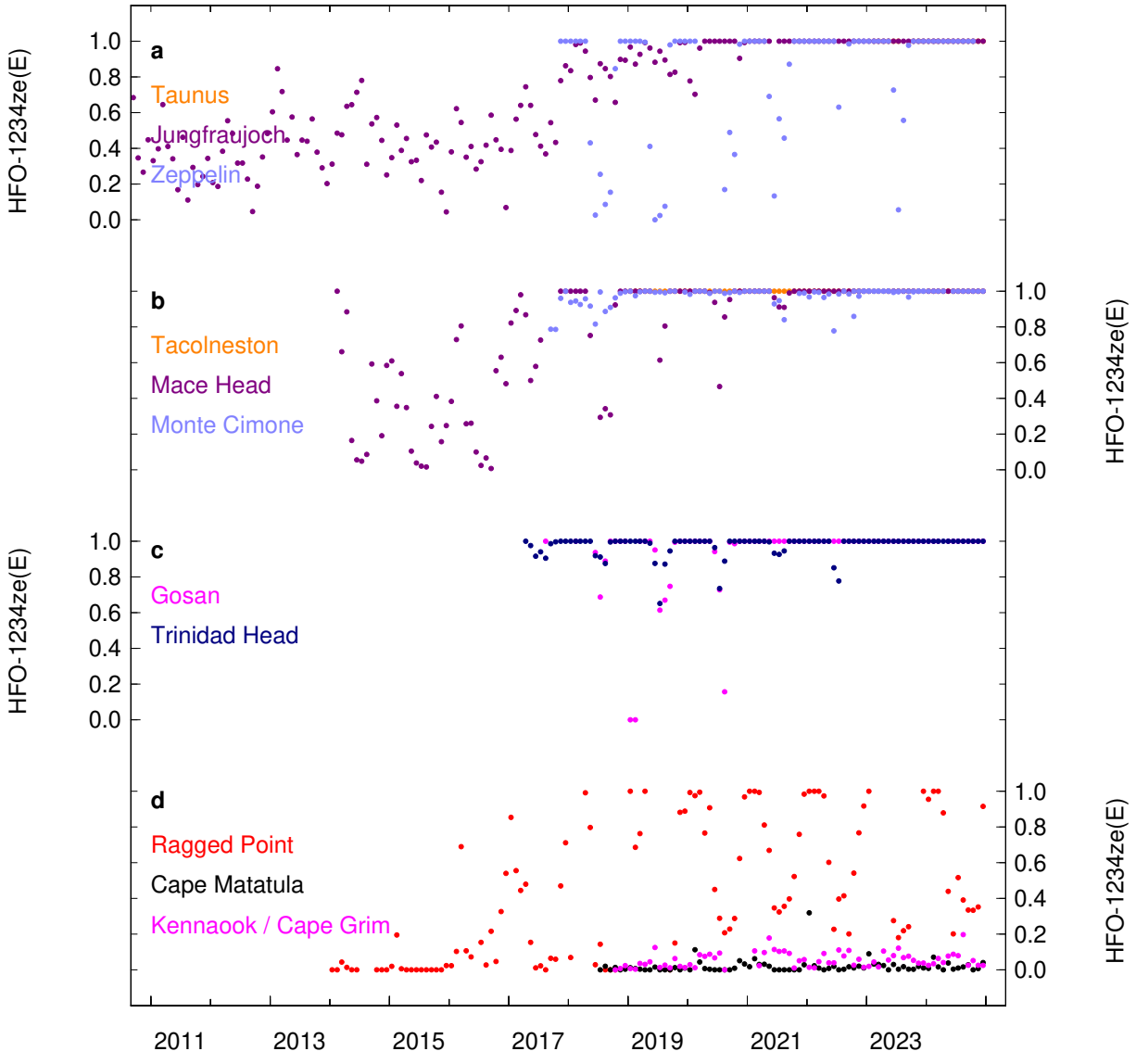

Figure A2. Ratio of the number of detectable to total measurements (monthly bins) for HFO-1234ze(E) from AGAGE stations.

https://doi.org/10.5194/egusphere-2025-4824
Preprint. Discussion started: 7 October 2025

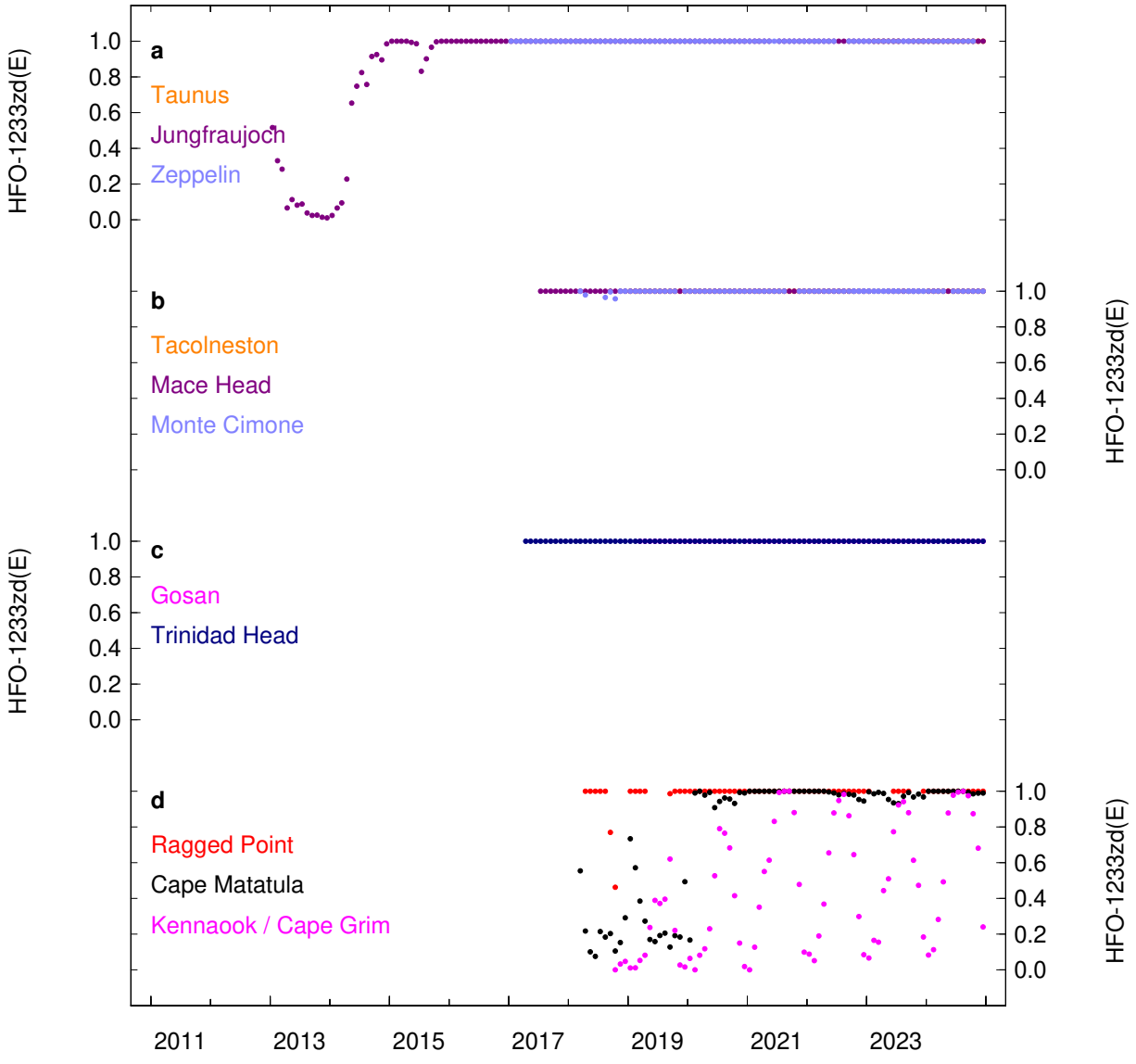

Figure A3. Ratio of the number of detectable to total measurements (monthly bins) for HCFO-1233zd(E) from AGAGE stations.

https://doi.org/10.5194/egusphere-2025-4824
Preprint. Discussion started: 7 October 2025

Appendix B: Comparison of the pollution ratios at selected sites

Using the observations at Jungfraujoch, Mace Head, and Gosan, we inspect the pollution events of the haloolefins and compare these to the pollution events of HFC-134a. The purpose of this comparison is to illustrate the gradual replacement of HFC-134a by the haloolefins.

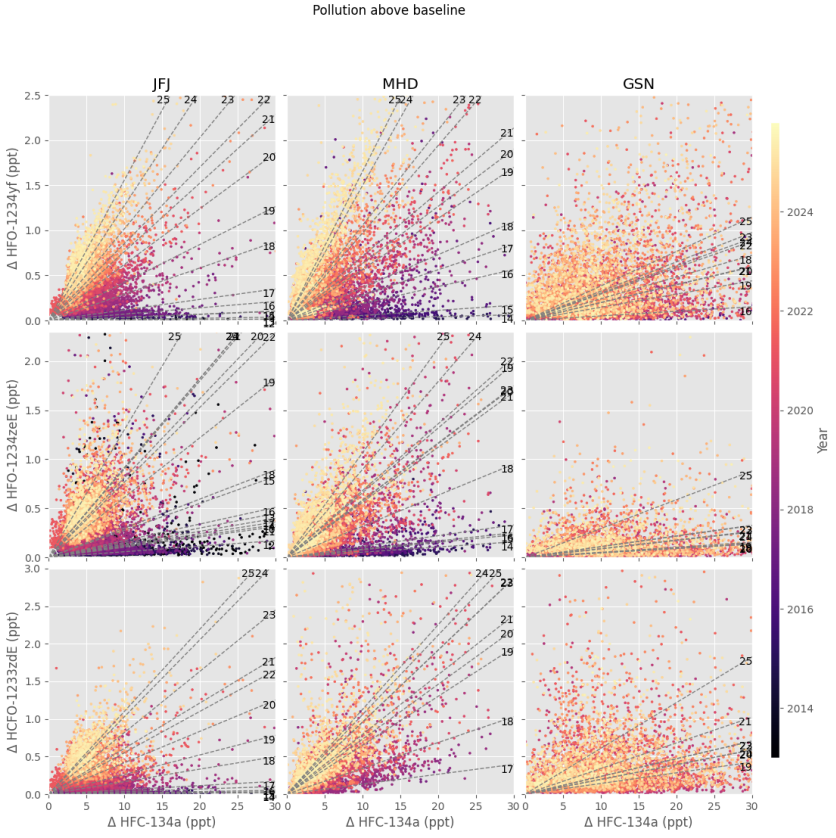

Figure B1. Pollution correlations against HFC-134a. Above-baseline (Δ) pollution mole fraction are determined for the haloolefins and HFC-134a using a baseline detection algorithm (Phyton pspline_arpls Erb, 2021; Baek et al., 2015). The slopes of yearly binned Δ haloolefins / Δ HFC-134a are determined by linear regression using least square fitting techniques (in y-dimension only, forced through 0/0). Numbers on the dashed lines for the linear regressions denote the years. These ratio slopes increase over time for all three haloolefins. See main text and Fig. 3 for further interpretations.

https://doi.org/10.5194/egusphere-2025-4824
Preprint. Discussion started: 7 October 2025

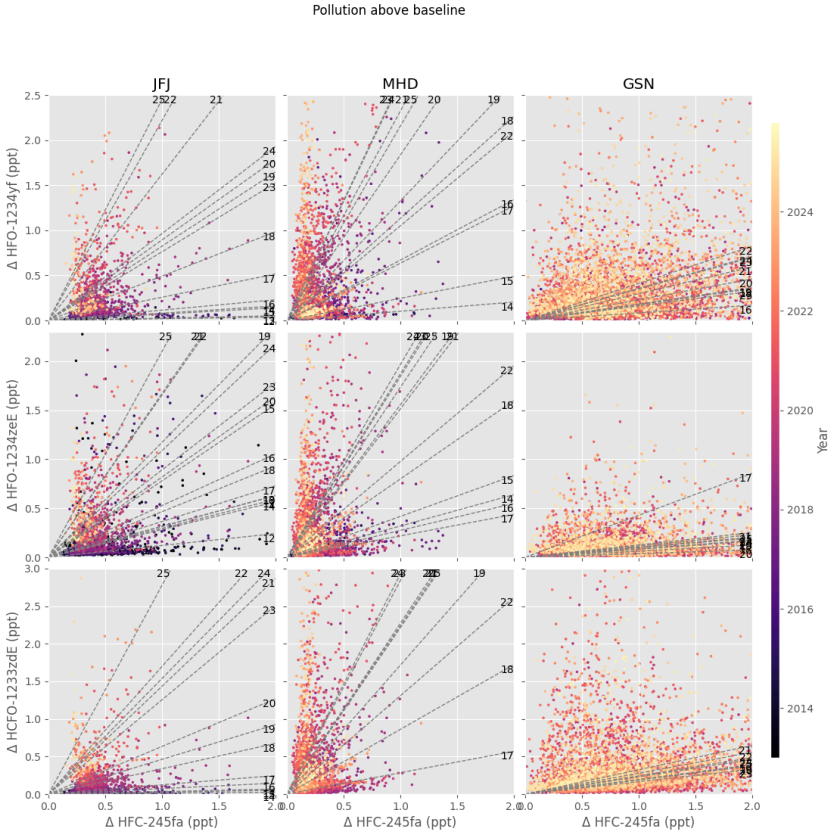

Figure B2. Pollution correlations against HFC-245fa. Above-baseline (Δ) pollution mole fraction are determined for the haloolefins and HFC-245fa using a baseline detection algorithm (Phyton pspline_arpls Erb, 2021; Baek et al., 2015). The slopes of yearly binned Δ haloolefins / Δ HFC-245fa are determined by linear regression using least square fitting techniques (in y-dimension only, forced through 0/0). Numbers on the dashed lines for the linear regressions denote the years. These ratio slopes increase over time for all three haloolefins. See main text and Fig. 3 for further interpretations.

https://doi.org/10.5194/egusphere-2025-4824
Preprint. Discussion started: 7 October 2025

Appendix C: Observations at King Sejong, Antarctica

Observations of the three haloolefins are also available from the measurements of samples collected weekly at the South Korean Antarctic station King Sejong, King George Island (South Shetland Islands) and analyzed at Empa (Vollmer et al., 2011). Air samples have been collected since 2007, but until 2012 the measurement program was not set to measure haloolefins. During 2012–2016 the measurements showed obvious contamination of unclear origin for HFO-1234yf and HFO-1234ze(E) and were thus discarded. Every year, batch analyses are conducted for these samples, however, the acquisitions of the three haloolefins is not activated for all samples to improve sensitivity and precision for chromatographically nearby eluting compounds. Results of the measurements are shown in Fig. C1 in comparison with in-situ results from Kennaook / Cape Grim and Cape Matatula (American Samoa). The yearly batch analyses are not following strict measurement protocol (in terms of analytical alternation with working standard measurements, analytical sample size) and mass spectrometric sensitivities are by nature not identical, such that peak detection levels may vary from year to year. Chromatographic peaks corresponding to mole fractions <10 ppq (parts-per-quadrillion, femtomol mol^{-1}) for HFO-1234yf and HFO-1234ze(E) and <5 ppq for HCFO-1233zd(E) are not reliably related to the presence of the substance in the sample. Hence, most measurements are deemed non-detectable. Despite the absence of the haloolefins in most samples, these results are potentially useful for future modeling approaches as they provide a limitation to the presence of these substances in the sampled region. While for HFO-1234yf and HFO-1234ze(E) the record shows occasional detectable mole fraction, for HCFO-1233zd(E), which is the longest-lived of the three haloolefins, a clear first appearance is detected, with an increasing number of detectable mole fractions over the last years, predominantly from samples collected during the austral winter. This is a first reported evidence that this compound has reached the Antarctic continent. Numeric results for the three compounds are provided as part of this study.

https://doi.org/10.5194/egusphere-2025-4824
Preprint. Discussion started: 7 October 2025

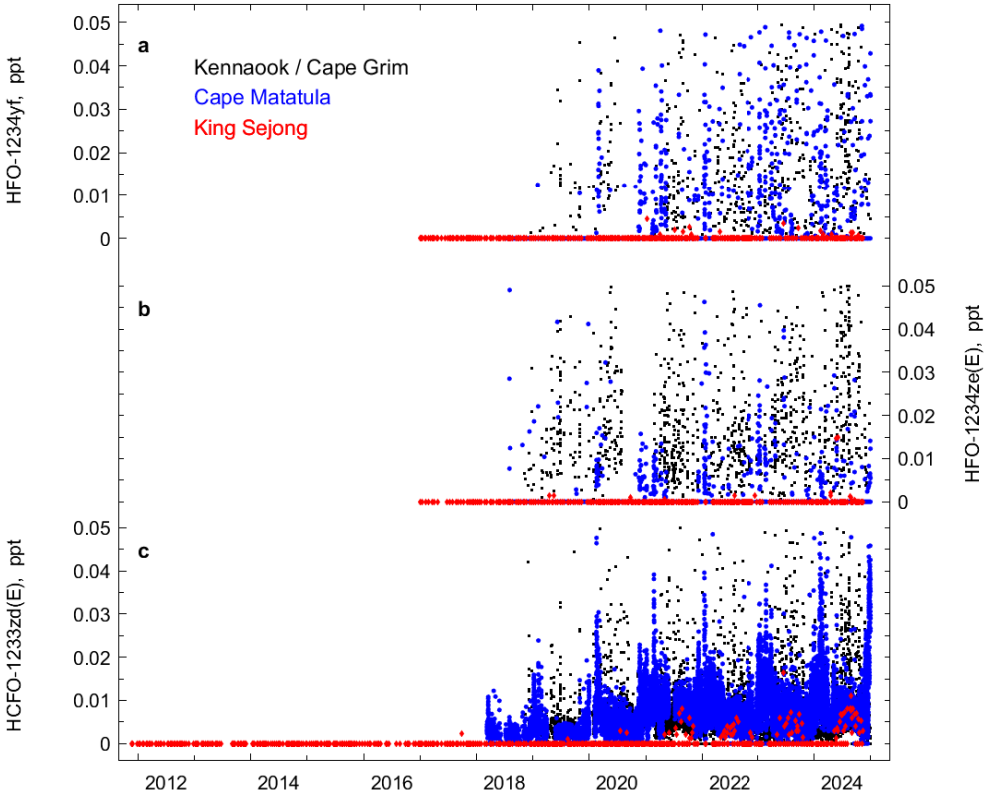

Figure C1. Observations of HFO-1234yf, HFO-1234ze(E) and HCFO-1233zd(E) from the South Korean Antarctic station King Sejong (red diamonds) compared to the in-situ records at Cape Matatula (blue circles) and Kennaook / Cape Grim (black squares). Mole fractions >0.05 ppt are omitted from this figure. Results show mostly non-detectable haloolefins but for HCFO-1233zd(E), some first detectable mole fractions are seen during the austral winter.

https://doi.org/10.5194/egusphere-2025-4824
Preprint. Discussion started: 7 October 2025

Appendix D: Effects of atmospheric lifetimes

The atmospheric lifetimes of HFO-1234yf, HFO-1234ze(E), and HCFO-1233zd(E) are considerably shorter than those of e.g., HFCs, hence an additional calculation is made to account for their degradation in the atmosphere over the model simulation. The rates of their atmospheric decay are based on calculations by Henne et al. (2012) using OH fields and FLEXPART simulations to derive HFO-1234yf monthly mean lifetimes. The resulting monthly mean lifetimes are given in Table D1 and are valid for a release in Europe. The effects of including lifetimes in the transport model on inverse emission estimates is shown in Fig. D1. It can be seen that a non-negligible bias in posterior emissions occurs when this atmospheric degradation is not accounted for, with the expected largest discrepancy for the shorter-lived HFO-1234yf and HFO-1234ze(E), and with less effect for the longer-lived HCFO-1233zd(E).

Table D1. Atmospheric lifetimes (in days) for HFO-1234yf ($CF_3CF{=}CH_2$), HFO-1234zeE (*trans*-$CF_3CH{=}CHF$), and HCFO-1233zdE (*trans*-$CF_3CH{=}CHCl$).

Compound	Jan	Feb	Mar	Apr	May	Jun	Jul	Aug	Sep	Oct	Nov	Dec
HFO-1234yf	35.6	24.3	14.1	7.8	4.8	3.6	3.7	4.7	7.9	14.9	30.8	41.8
HFO-1234ze(E)	56.3	38.4	22.3	12.3	7.7	5.7	5.9	7.4	12.4	23.5	48.8	66.1
HCFO-1233zd(E)	125.6	85.7	49.8	27.5	17.1	12.8	13.2	16.5	27.8	52.5	108.9	147.6

https://doi.org/10.5194/egusphere-2025-4824
Preprint. Discussion started: 7 October 2025

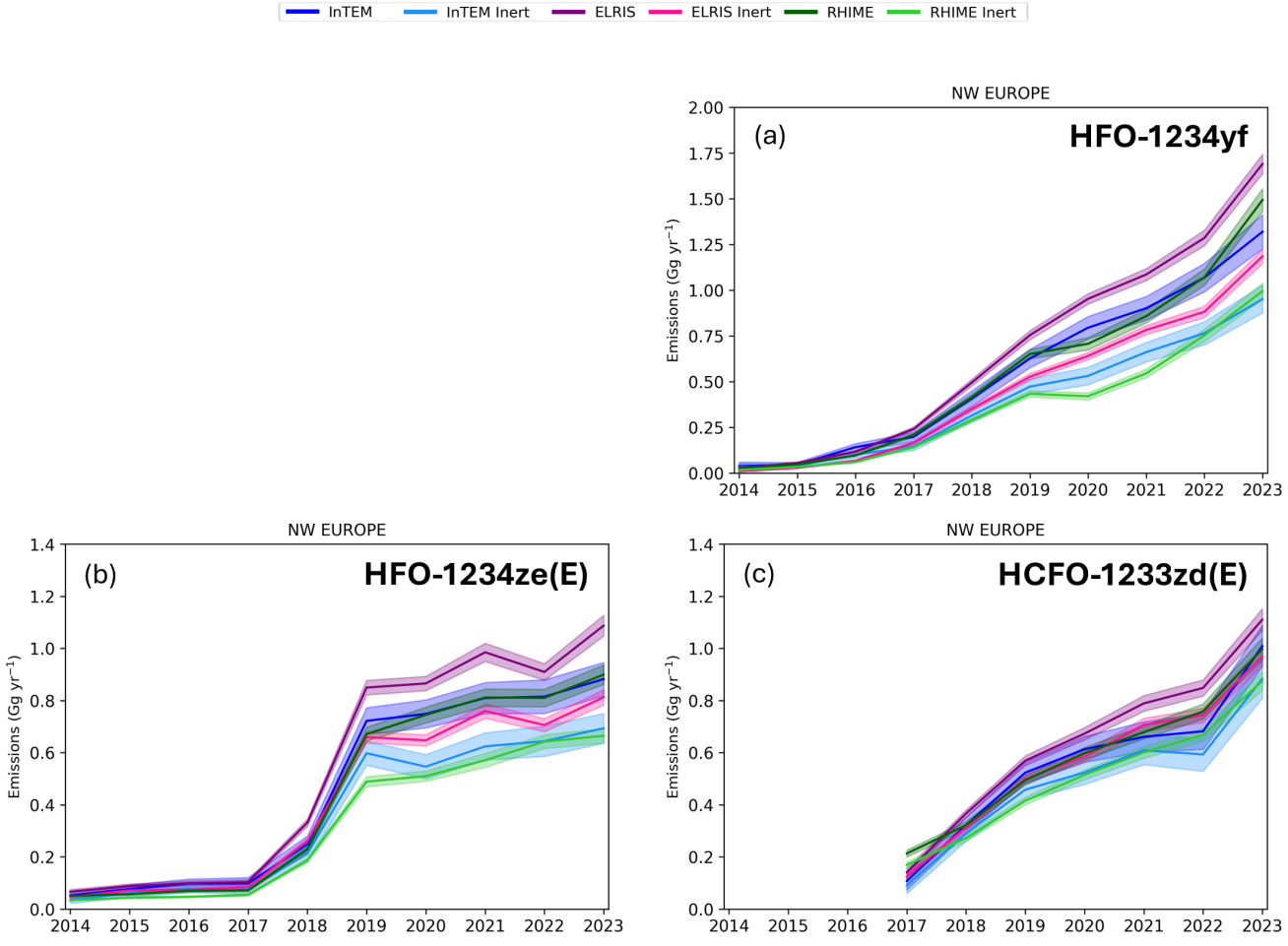

Figure D1. Comparison of emissions of (a) HFO-1234yf, (b) HFO-1234ze(E) and (c) HCFO-1233zd(E) from NW Europe for the lifetimes used in this work versus inertness. Significant differences for the two approaches demonstrate the need to include degradation/lifetime in the inverse methods approach.

https://doi.org/10.5194/egusphere-2025-4824
Preprint. Discussion started: 7 October 2025

Appendix E: Prior flux sensitivity test

A sensitivity test was conducted to evaluate the impact of the spatial distribution of prior fluxes on the posterior emission estimates. Two prior flux maps were used: the first was the base case where emissions were distributed by population density, and the second was a flat prior where emissions were uniformly distributed over the land surface. In both cases the emissions were scaled to produce a total annual emission of 1 Gg for NW Europe. The posterior emission estimates using both prior maps are shown as timeseries in Fig. E1 and as spatial distributions in Fig. E2. It can be seen that the choice of prior has a minimal impact on the posterior emissions for all three models.

https://doi.org/10.5194/egusphere-2025-4824
Preprint. Discussion started: 7 October 2025

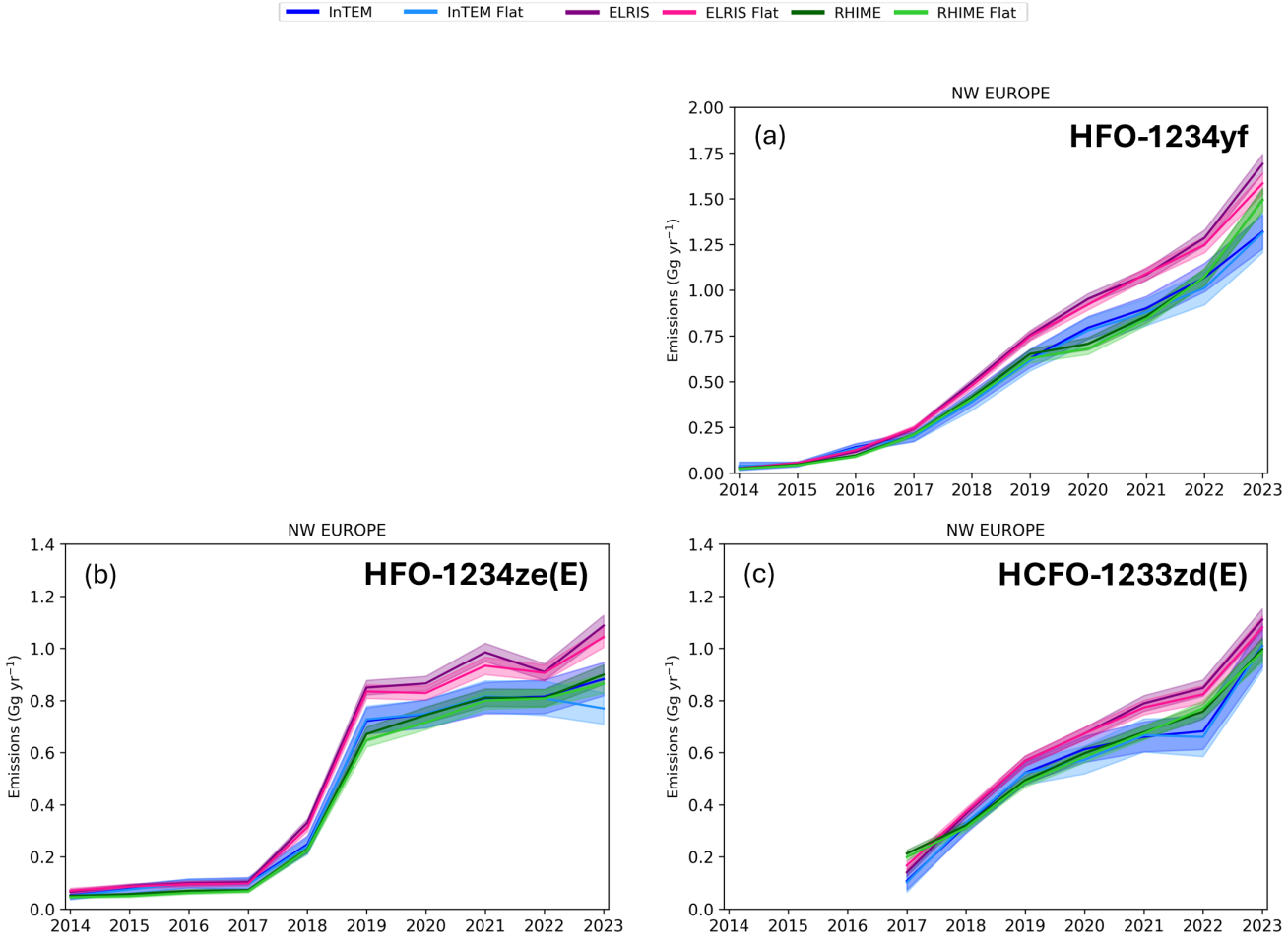

Figure E1. Impact of prior emission distribution for (a) HFO-1234yf, (b) HFO-1234ze(E) and (c) HCFO-1233zd(E) on posterior NW Europe emissions. Here the base case (using a population prior) is compared with the use of a flat land prior. Total posterior emissions for a given model do not have a significant dependence on the prior spatial distribution.

https://doi.org/10.5194/egusphere-2025-4824
Preprint. Discussion started: 7 October 2025

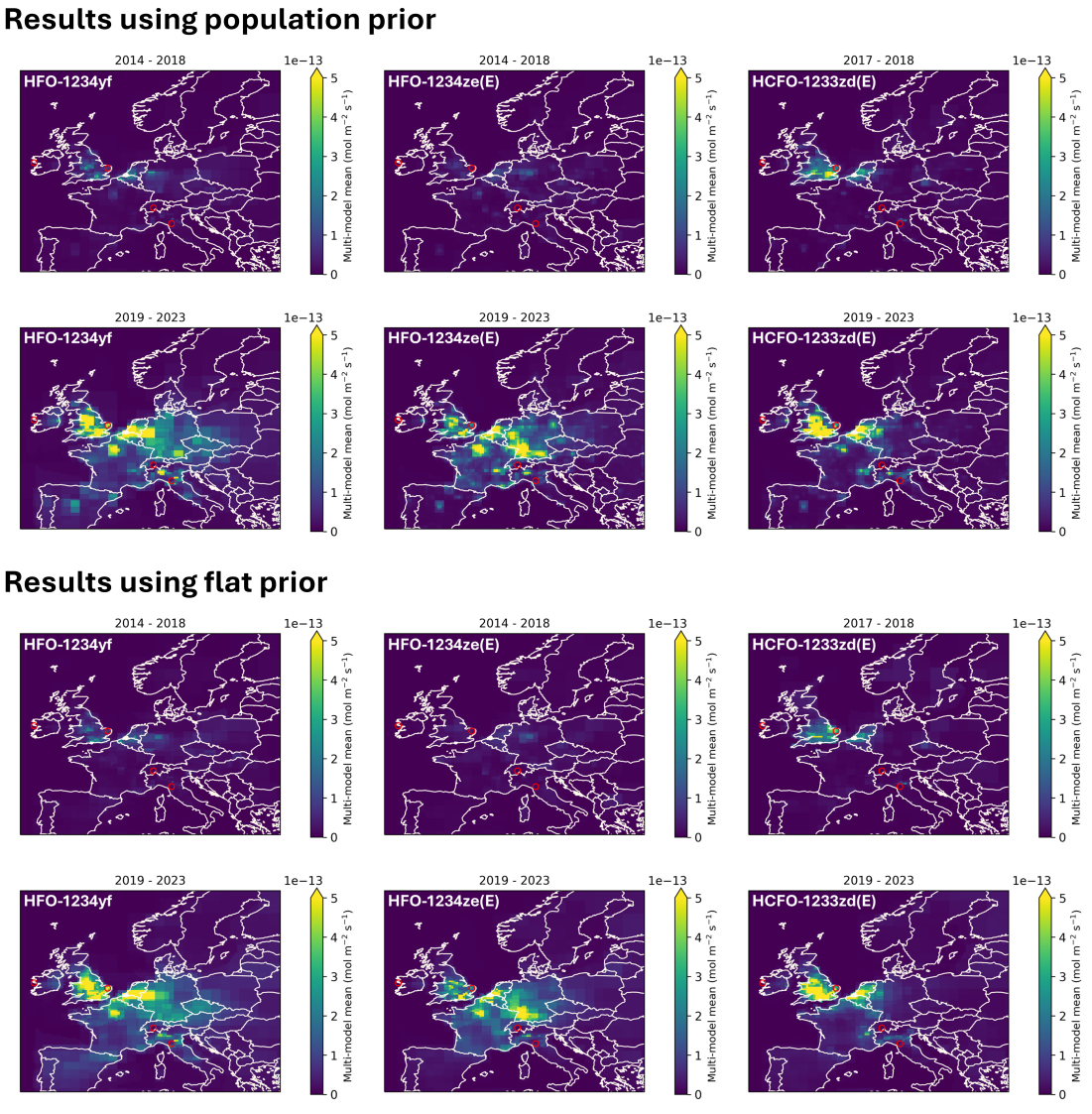

Figure E2. Spatial distribution maps for Northwest (NW) European comparing the population-based and the flat priors. Emissive fluxes of HFO-1234yf, HFO-1234ze(E) and HCFO-1233zd(E) for the periods 2014–2018 (2017–2018 for HCFO-1233zd(E)) in the respective upper panels and for 2019–2023 in the lower panels. Red circles denote measurement sites and are, from west to east, Mace Head (Ireland), Tacolneston (UK), Jungfraujoch (Switzerland), and Monte Cimone (Italy).

https://doi.org/10.5194/egusphere-2025-4824
Preprint. Discussion started: 7 October 2025

Appendix F: Emissions for individual countries

Emissions are shown for the individual countries/regions UK (Fig. F1), France (Fig. F2), Germany (Fig. F3), and the Benelux countries (Belgium, The Netherlands, and Luxembourg, Fig. F4).

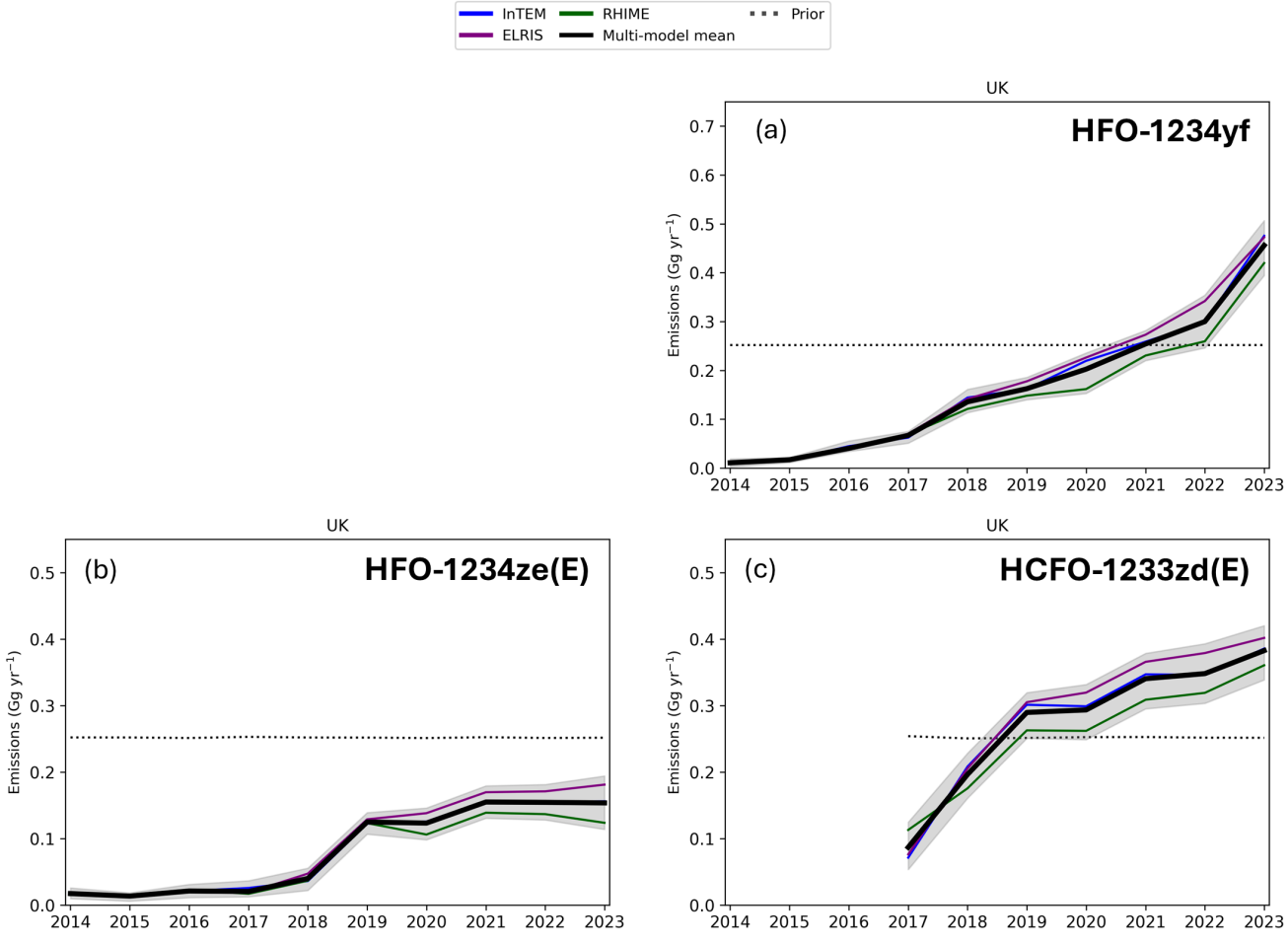

Figure F1. Emissions of HFO-1234yf, HFO-1234ze(E), and HCFO-1233zd(E) from the United Kingdom (UK), including England, Scotland, Wales and Northern Ireland. Emissions are shown for the three model approaches InTEM, ELRIS, and RHIME and for their mean, including an uncertainty for that mean (see Fig. 6 for details).

https://doi.org/10.5194/egusphere-2025-4824
Preprint. Discussion started: 7 October 2025

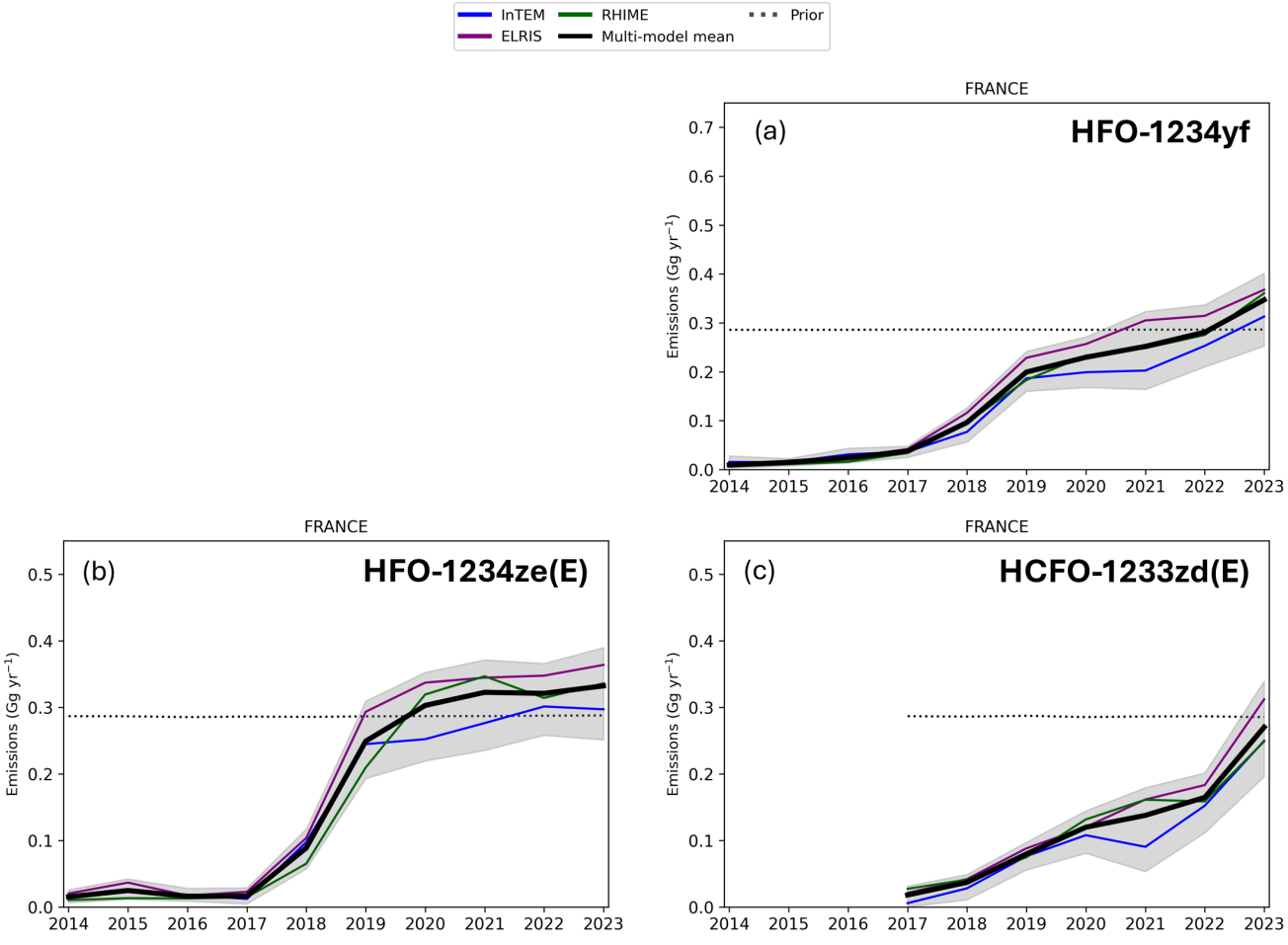

Figure F2. Emissions of HFO-1234yf, HFO-1234ze(E), and HCFO-1233zd(E) from France (see Fig. 6 for details).

https://doi.org/10.5194/egusphere-2025-4824
Preprint. Discussion started: 7 October 2025

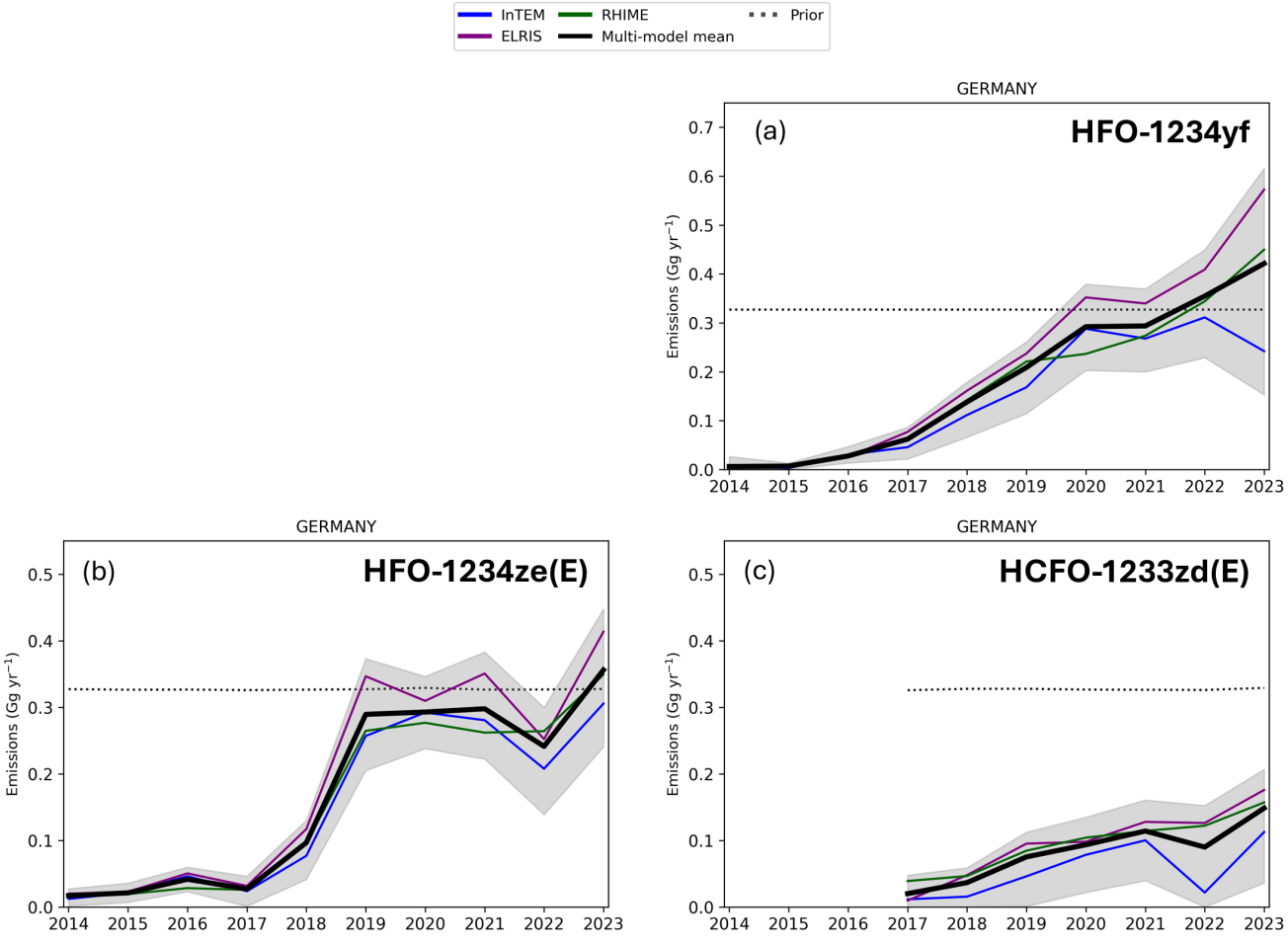

Figure F3. Emissions of HFO-1234yf, HFO-1234ze(E), and HCFO-1233zd(E) from Germany (see Fig. 6 for details).

https://doi.org/10.5194/egusphere-2025-4824
Preprint. Discussion started: 7 October 2025

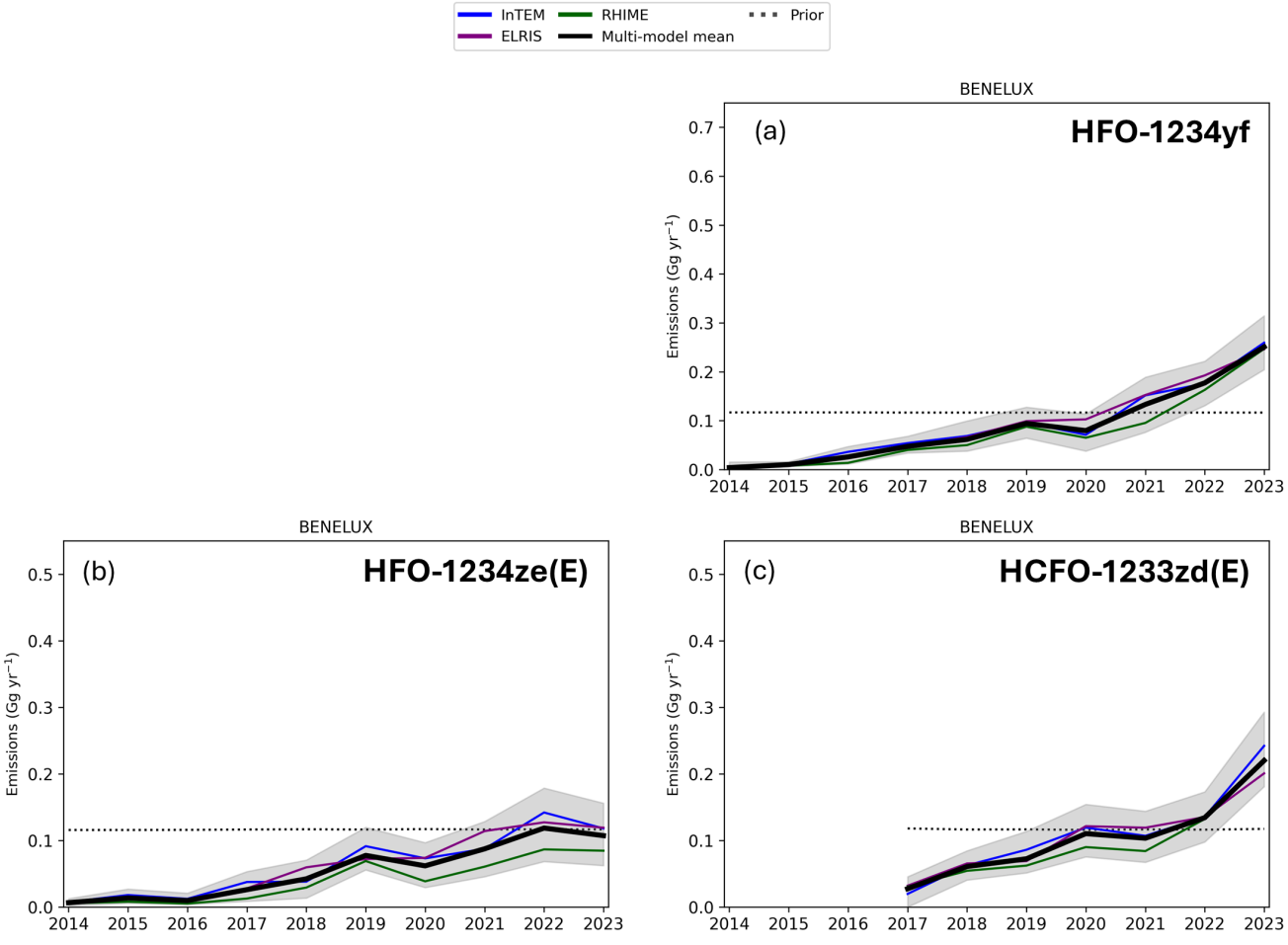

Figure F4. Emissions of HFO-1234yf, HFO-1234ze(E), and HCFO-1233zd(E) from the Benelux countries (see Fig. 6 for details).

https://doi.org/10.5194/egusphere-2025-4824
Preprint. Discussion started: 7 October 2025

References

Arnold, T., Mühle, J., Salameh, P. K., Harth, C. M., Ivy, D. J., and Weiss, R. F.: Automated Measurement of Nitrogen Trifluoride in Ambient Air, Anal. Chem., 84, 4798–4804, https://doi.org/10.1021/ac300373e, 2012.

Arnold, T., Manning, A. J., Kim, J., Li, S., Webster, H., Thomson, D., Mühle, J., Weiss, R. F., Park, S., and O'Doherty, S.: Inverse modelling of CF_4 and NF_3 emissions in East Asia, Atmos. Chem. Phys., 18, 13 305–13 320, https://doi.org/10.5194/acp-18-13305-2018, 2018.

Arp, H. P. H., Gredelj, A., Glüge, J., Scheringer, M., and Cousins, I. T.: The global threat from the irreversible accumulation of trifluoroacetic acid (TFA), Environ. Sci. Technol., 58, 19 925–19 935, https://doi.org/10.1021/acs.est.4c06189, 2024.

Baek, S.-J., Park, A., Ahn, Y.-J., and Choo, J.: Baseline correction using asymmetrically reweighted penalized least squares smoothing, Analyst, 140, 250–257, https://doi.org/10.1039/C4AN01061B, 2015.

Behringer, D., Heydel, F., Gschrey, B., Osterheld, S., Schwarz, W., Warncke, K., Freeling, F., Nödler, K., Henne, S., Reimann, S., Blepp, M., Jörß, W., Liu, R., Ludig, S., Rüdenauer, I., and Gartiser, S.: Persistent degradation products of halogenated refrigerants and blowing agents in the environment: type, environmental concentrations, and fate with particular regard to new halogenated substitutes with low global warming potential, Tech. Rep. FB000452/ENG, German Environment Agency, 2021.

Berchet, A., Pison, I., Chevallier, F., Bousquet, P., Conil, S., Geever, M., Laurila, T., Lavrič, J., Lopez, M., Moncrieff, J., Necki, J., Ramonet, M., Schmidt, M., Steinbacher, M., and Tarniewicz, J.: Towards better error statistics for atmospheric inversions of methane surface fluxes, Atmos. Chem. Phys., 13, 7115–7132, https://doi.org/10.5194/acp-13-7115-2013, 2013.

Bey, I., Jacob, D. J., Yantosca, R. M., Logan, J. A., Field, B. D., Fiore, A. M., Li, Q., Liu, H. Y., Mickley, L. J., and Schultz, M. G.: Global modeling of tropospheric chemistry with assimilated meteorology: Model description and evaluation, J. Geophys. Res. Atmos., 106, 23 073–23 095, https://doi.org/https://doi.org/10.1029/2001JD000807, 2001.

Burkholder, J. and Hodnebrog, Ø.: Annex: Summary of Abundances, Lifetimes, ODPs, REs, GWPs, and GTPs, Appendix A, in: Scientific Assessment of Ozone Depletion: 2022, Global Ozone Research and Monitoring Project — Report No. 278, World Meteorological Organization, Geneva, 2022.

Choi, H., Redington, A. L., Park, H., Kim, J., Thompson, R. L., Mühle, J., Salameh, P. K., Harth, C. M., Weiss, R. F., Manning, A. J., and Park, S.: Revealing the significant acceleration of hydrofluorocarbon (HFC) emissions in eastern Asia through long-term atmospheric observations, Atmos. Chem. Phys., 24, 7309–7330, https://doi.org/10.5194/acp-24-7309-2024, 2024.

Cunnold, D. M., Prinn, R. G., Rasmussen, R. A., Simmonds, P. G., Alyea, F. N., Cardelino, C. A., Crawford, A. J., Fraser, P. J., and Rosen, R. D.: The atmospheric lifetime experiment: 3. Lifetime methodology and application to 3 years of $CFCl_3$ data, J. Geophys. Res., 88, 8379–8400, https://doi.org/10.1029/JC088iC13p08379, 1983.

David, L. M., Barth, M., Höglund-Isaksson, L., Purohit, P., Velders, G. J. M., Glaser, S., and Ravishankara, A. R.: Trifluoroacetic acid deposition from emissions of HFO-1234yf in India, China, and the Middle East, Atmos. Chem. Phys., 21, 14 833–14 849, https://doi.org/10.5194/acp-21-14833-2021, 2021.

Erb, D.: pybaselines: A Python library of algorithms for the baseline correction of experimental data, https://doi.org/10.5281/zenodo.5608581, 2021.

European Chemicals Agency: Background Document to the Opinion on the Annex XV dossier proposing restrictions on Per- and polyfluoroalkyl substances (PFASs), https://echa.europa.eu/hot-topics/perfluoroalkyl-chemicals-pfas, , 2024.

https://doi.org/10.5194/egusphere-2025-4824
Preprint. Discussion started: 7 October 2025

European Parliament and Council: Directive 2006/40/EC of the European Parliament and of the Council of 17 May 2006 relating to emissions from air conditioning systems in motor vehicles and amending Council Directive 70/156/EEC (Text with EEA relevance), https://eur-lex.europa.eu/eli/dir/2006/40/oj, Document 32006L0040, MAC directive EU, 2006.

European Parliament and Council: Regulation (EU) No 517/2014 of the European Parliament and of the Council of 16 April 2014 on fluorinated greenhouse gases, and repealing Regulation (EC) No 842/2006, https://eur-lex.europa.eu/legal-content/EN/TXT/?uri=uriserv:OJ.L_.2014.150.01.0195.01.ENG, 2014 F-gas regulation, last accessed 2025-08-29, 2014.

European Parliament and Council: Regulation (EU) 2024/573 of the European Parliament and of the Council of 7 February 2024 on fluorinated greenhouse gases, amending Directive (EU) 2019/1937 and repealing Regulation (EU) No 517/2014, https://eur-lex.europa.eu/eli/reg/2024/573/oj, 2024 F-gas regulation, last accessed 2025-07-03, 2024.

EUROSTAT: Road transport equipment - stock of vehicles - Passenger cars, by type of motor energy, https://doi.org/10.2908/ROAD_EQS_CARPDA, 2025a.

EUROSTAT: Population (national level) - Population on 1 January, https://doi.org/10.2908/TPS00001, 2025b.

Ganesan, A. L., Rigby, M., Zammit-Mangion, A., Manning, A. J., Prinn, R. G., Fraser, P. J., Harth, C. M., Kim, K.-R., Krummel, P. B., Li, S., Mühle, J., O'Doherty, S. J., Park, S., Salameh, P. K., Steele, L. P., and Weiss, R. F.: Characterization of uncertainties in atmospheric trace gas inversions using hierarchical Bayesian methods, Atmospheric Chemistry and Physics, 14, 3855–3864, https://doi.org/10.5194/acp-14-3855-2014, 2014.

Ganesan, A. L., Manizza, M., Morgan, E. J., Harth, C. M., Kozlova, E., Lueker, T., Manning, A. J., Lunt, M. F., Mühle, J., Lavric, J. V., Heimann, M., Weiss, R. F., and Rigby, M.: Marine Nitrous Oxide Emissions From Three Eastern Boundary Upwelling Systems Inferred From Atmospheric Observations, Geophys. Res. Lett., 47, e2020GL087 822, https://doi.org/https://doi.org/10.1029/2020GL087822, e2020GL087822 2020GL087822, 2020.

GEOS-Chem: https://doi.org/10.5281/zenodo.10034733, 2023.

Guillevic, M., Vollmer, M. K., Wyss, S. A., Leuenberger, D., Ackermann, A., Pascale, C., Niederhauser, B., and Reimann, S.: Dynamic–gravimetric preparation of metrologically traceable primary calibration standards for halogenated greenhouse gases, Atmos. Meas. Tech., 11, 3351–3372, https://doi.org/10.5194/amt-11-3351-2018, 2018.

Hart, L., Hossaini, R., Wild, O., Halsall, C., Mazzeo, A., Hou, X., Wang, Z., Chipperfield, M. P., Arduini, J., Krummel, P. B., Lunder, C. R., Mühle, J., O'Doherty, S., Park, S., Reimann, S., Stanley, K. M., and Young, D.: Growth in production and environmental deposition of trifluoroacetic acid due to Long-lived CFC replacements and anaesthetics, Geophys. Res. Lett., in review, 2025.

Henne, S., Shallcross, D. E., Reimann, S., Xiao, P., Brunner, D., O'Doherty, S., and Buchmann, B.: Future emissions and atmospheric fate of HFC-1234yf from mobile air conditioners in Europe, Environ. Sci. Technol., 46, 1650–1658, https://doi.org/10.1021/es2034608, 2012.

Henne, S., Brunner, D., Oney, B., Leuenberger, M., Eugster, W., Bamberger, I., Meinhardt, F., Steinbacher, M., and Emmenegger, L.: Validation of the Swiss methane emission inventory by atmospheric observations and inverse modelling, Atmospheric Chemistry and Physics, 16, 3683–3710, https://doi.org/10.5194/acp-16-3683-2016, 2016.

Henne, S., Storck, F. R., Wöhrnschimmel, H., Leuenberger, M., Vollmer, M. K., and Reimann, S.: Trifluoroacetate (TFA) in Precipitation and Surface Waters in Switzerland: Trends, Source Attribution, and Budget, EGUsphere, 2025, 1–43, https://doi.org/10.5194/egusphere-2025-2861, 2025.

Holland, R., Khan, M. A. H., Driscoll, I., Chhantyal-Pun, R., Derwent, R. G., Taatjes, C. A., Orr-Ewing, A. J., Percival, C. J., and Shallcross, D. E.: Investigation of the production of trifluoroacetic acid from two halocarbons, HFC-134a and HFO-1234yf and its fates using a global

https://doi.org/10.5194/egusphere-2025-4824
Preprint. Discussion started: 7 October 2025

three-dimensional chemical transport model, ACS Earth Space Chem., 5, 849–857, https://doi.org/10.1021/acsearthspacechem.0c00355, 2021.

Jones, A., Thomson, D., Hort, M., and Devenish, B.: The U.K. Met Office's next-generation atmospheric dispersion model, NAME III, in Borrego C. and Norman A.-L. (Eds), Air Pollution Modeling and its Application XVII (Proceedings of the 27th NATO/CCMS International Technical Meeting on Air Pollution Modelling and its Application), Springer, pp. 580–589, 2007.

Katharopoulos, I., Rust, D., Vollmer, M. K., Brunner, D., Reimann, S., O'Doherty, S. J., Young, D., Stanley, K. M., Schuck, T., Arduini, J., Emmenegger, L., and Henne, S.: Impact of transport model resolution and a priori assumptions on inverse modeling of Swiss F-gas emissions, Atmos. Chem. Phys., 23, 14 159–14 186, https://doi.org/10.5194/acp-23-14159-2023, 2023.

Khan, M. A. H., Mendes, D., Holland, R., de Los Angeles Garavagno, M., Orr-Ewing, A., Stanley, K., O'Doherty, S., Young, D., Vollmer, M. K., Antony, A. J., Karamshahi, F., Percival, C. J., Bacak, A., Derwent, R. G., and Shallcross, D. E.: Trifluoroacetic acid surface concentration and deposition estimates generated from the gas-phase oxidation of a wide range of precursor hydrofluoroolefins, Environmental Science: Atmospheres, in review, xx–xx, 2025.

Liang, Q., Rigby, M., Fang, X., Godwin, D., Müle, J., Saito, T., Stanley, K. M., and Velders, G. J. M.: Update on Ozone-Depleting Substances (ODSs) and Other Gases of Interest to the Montreal Protocol, Chapter 2, in: Scientific Assessment of Ozone Depletion: 2022, Global Ozone Research and Monitoring Project — Report No. 278, p. 509, World Meteorological Organization, Geneva, 2022.

Lindley, A., McCulloch, A., and Vink, T.: Contribution of hydrofluorocarbons (HFCs) and hydrofluoro-olefins (HFOs) atmospheric breakdown products to acidification ("acid rain") in the EU at present and in the future, Open J. Air Pollut, 8, 81–95, https://doi.org/10.4236/ojap.2019.84004, 2019.

Madronich, S., Sulzberber, B., Longstreth, J. D., Schikowski, T., Andersen, M. P. S., Solomon, K. R., and Wilson, S. R.: Changes in tropospheric air quality related to the protection of stratospheric ozone in a changing climate, Photochem Photobiol Sci, 22, 1129–1176, https://doi.org/10.1007/s43630-023-00369-6, 2023.

Maione, M., Giostra, U., Arduini, J., Furlani, F., Graziosi, F., Lo Vullo, E., and Bonasoni, P.: Ten years of continuous observations of stratospheric ozone depleting gases at Monte Cimone (Italy) — Comments on the effectiveness of the Montreal Protocol from a regional perspective, Sci. Tot. Environ., pp. 155–164, https://doi.org/10.1016/j.scitotenv.2012.12.056, 2013.

Manning, A. J., Redington, A. L., Say, D., O'Doherty, S., Young, D., Simmonds, P. G., Vollmer, M. K., Mühle, J., Arduini, J., Spain, G., Wisher, A., Maione, M., Schuck, T. J., Stanley, K., Reimann, S., Engel, A., Krummel, P. B., Fraser, P. J., Harth, C. M., Salameh, P. K., Weiss, R. F., Gluckman, R., Brown, P. N., Watterson, J. D., and Arnold, T.: Evidence of a recent decline in UK emissions of hydrofluorocarbons determined by the InTEM inverse model and atmospheric measurements, Atmos. Chem. Phys., 21, 12 739–12 755, https://doi.org/10.5194/acp-21-12739-2021, 2021.

McGillen, M. R., Fried, Z. T. P., Khan, M. A. H., Kuwata, K. T., Martin, C. M., O'Doherty, S., Pecere, F., Shallcross, D. E., Stanley, K. M., and Zhang, K.: Ozonolysis can produce long-lived greenhouse gases from commercial refrigerants, Proc. Natl. Acad. Sci. USA, 120, https://doi.org/10.1073/pnas.2312714120, 2023.

Meixner, K., Wagenhäuser, T., Schuck, T. J. Redington, A. L., Stanley, K. M., O'Doherty, S., Young, D., Pitt, J., Wenger, A., Frumau, A., Stavert, A. R., Rennick, C., Vollmer, M. K., Maione, M., Arduini, J., Lunder, C. R., Couret, C., Jordan, A., Guitèrrez, X., Kubistin, D., Mueller-Williams, J., Lindauer, M., Vojta, M., Stohl, A., and Engel, A.: Characterisation of German SF_6 emissions, Environ. Sci. Technol., in review, 2025.

https://doi.org/10.5194/egusphere-2025-4824
Preprint. Discussion started: 7 October 2025

Miller, B. R., Weiss, R. F., Salameh, P. K., Tanhua, T., Greally, B. R., Mühle, J., and Simmonds, P. G.: Medusa: A sample preconcentration and GC/MS detector system for in situ measurements of atmospheric trace halocarbons, hydrocarbons, and sulfur compounds, Anal. Chem., 80, 1536–1545, https://doi.org/10.1021/ac702084k, 2008.

Nielsen, O. J., Javadi, M. S., Sulbaek Andersen, M. P., Hurley, M. D., Wallington, T. J., and Singh, R.: Atmospheric chemistry of $CF_3CF{=}CH_2$: kinetics and mechanisms of gas-phase reactions with Cl atoms, OH radicals, and O_3, Chem. Phys. Lett., 439, 18–22, https://doi.org/10.1016/j.cplett.2007.03.053, 2007.

O'Doherty, S., Cunnold, D. M., Manning, A., Miller, B. R., Wang, R. H. J., Krummel, P. B., Fraser, P. J., Simmonds, P. G., McCulloch, A., Weiss, R. F., Salameh, P., Porter, L. W., Prinn, R. G., Huang, J., Sturrock, G., Ryall, D., Derwent, R. G., and Montzka, S. A.: Rapid growth of hydrofluorocarbon 134a and hydrochlorofluorocarbons 141b, 142b, and 22 from Advanced Global Atmospheric Gases Experiment (AGAGE) observations at Cape Grim, Tasmania, and Mace Head, Ireland, J. Geophys. Res., 109, https://doi.org/10.1029/2003JD004277, 2004.

Pérez-Peña, M. P., Fisher, J. A., Hansen, C., and Kable, S. H.: Assessing the atmospheric fate of trifluoroacetaldehyde (CF_3CHO) and its potential as a new source of fluoroform (HFC-23) using the AtChem2 box model, Environ. Sci.: Atmos., 3, 1767–1777, https://doi.org/10.1039/d3ea00120b, 2023.

Prinn, R. G., Weiss, R. F., Arduini, J., Arnold, T., DeWitt, H. L., Fraser, P. J., Ganesan, A. L., Gasore, J., Harth, C. M., Hermansen, O., Kim, J., Krummel, P. B., Li, S., Loh, Z. M., Lunder, C. R., Maione, M., Manning, A. J., Miller, B. R., Mitrevski, B., Mühle, J., O'Doherty, S., Park, S., Reimann, S., Rigby, M., Saito, T., Salameh, P. K., Schmidt, R., Simmonds, P. G., Steele, L. P., Vollmer, M. K., Wang, R. H., Yao, B., Yokouchi, Y., Young, D., and Zhou, L.: History of chemically and radiatively important atmospheric gases from the Advanced Global Atmospheric Gases Experiment (AGAGE), Earth Syst. Sci. Data, 10, 985–1018, https://doi.org/10.5194/essd-10-985-2018, 2018.

Ramsden, A., Danjou, A., De Longueville, H., Melo, D. B., Constantin, L., Thanwerdas, J., Henne, S., and Bruch, V.: fluxy, https://github.com/openghg/fluxy, 2025.

Redington, A. L., Manning, A. J., Henne, S., Graziosi, F., Western, L. M., Arduini, J., Ganesan, A. L., Harth, C. M., Maione, M., Mühle, J., O'Doherty, S., Pitt, J., Reimann, S., Rigby, M., Salameh, P. K., Simmonds, P. G., Spain, T. G., Stanley, K., Vollmer, M. K., Weiss, R. F., and Young, D.: Western European Emission Estimates of CFC-11, CFC-12 and CCl_4 Derived from Atmospheric Measurements from 2008 to 2021, Atmos. Chem. Phys., 23, 7383–7398, https://doi.org/10.5194/acp-23-7383-2023, 2023.

Rigby, M., Prinn, R. G., O'Doherty, S., Montzka, S. A., McCulloch, A., Harth, C. M., Mühle, J., Salameh, P. K., Weiss, R. F., Young, D., Simmonds, P. G., Hall, B. D., Dutton, G. S., Nance, D., Mondeel, D. J., Elkins, J. W., Krummel, P. B., Steele, L. P., and Fraser, P. J.: Re-evaluation of lifetimes of the major CFCs and CH_3CCl_3 using atmospheric trends, Atmos. Chem. Phys., 13, 2691–2702, https://doi.org/10.5194/acp-13-2691-2013, 2013.

Ruckstuhl, A. F., Henne, S., Reimann, S., Steinbacher, M., Vollmer, M. K., O'Doherty, S., Buchmann, B., and Hueglin, C.: Robust extraction of baseline signal of atmospheric trace species using local regression, Atmos. Meas. Tech., 5, 2613–2624, https://doi.org/10.5194/amt-5-2613-2012, 2012.

Say, D., Kuyper, B., Western, L., Khan, M. A. H., Lesch, T., Labuschagne, C., Martin, D., Young, D., Manning, A. J., O'Doherty, S., Rigby, M., Krummel, P. B., Davies-Coleman, M. T., Ganesan, A. L., and Shallcross, D. E.: Emissions and Marine Boundary Layer Concentrations of Unregulated Chlorocarbons Measured at Cape Point, South Africa, Environ. Sci. Technol., 54, 10 514–10 523, https://doi.org/10.1021/acs.est.0c02057, 2020.

Sicard, A. J. and Baker, R. T.: Fluorocarbon Refrigerants and their Syntheses: Past to Present, Chem. Rev., 120, 9164–9303, https://doi.org/10.1021/acs.chemrev.9b00719, 2020.

https://doi.org/10.5194/egusphere-2025-4824
Preprint. Discussion started: 7 October 2025

Solomon, S., Alcamo, J., and Ravishankara, A. R.: Unfinished business after five decades of ozone-layer science and policy, Nat Commun, 11, https://doi.org/10.1038/s41467-020-18052-0, 2020.

Søndergaard, R., Nielsen, O. J., Hurley, M. D., Wallington, T. J., and Singh, R.: Atmospheric chemistry of trans-CF_3CH=CHF: kinetics of the gas-phase reactions with Cl atoms, OH radicals, and O_3, Chem. Phys. Lett., 443, 199–204, https://doi.org/10.1016/j.cplett.2007.06.084, 2007.

Steiner, M., Cantarello, L., Henne, S., and Brunner, D.: Flow-dependent observation errors for greenhouse gas inversions in an ensemble Kalman smoother, Atmos. Chem. Phys., 24, 12 447–12 463, https://doi.org/10.5194/acp-24-12447-2024, 2024.

Sulbaek Andersen, M. P. and Nielsen, O. J.: Tropospheric photolysis of CF_3CHO, Atmos. Environ., 272, https://doi.org/10.1016/j.atmosenv.2021.118935, 2022.

Sulbaek Andersen, M. P., Nilsson, E. J. K., Nielsen, O. J., Johnson, M. S., Hurley, M. D., and Wallington, T. J.: Atmospheric chemistry of trans-CF_3CH=CHCl: Kinetics of the gas-phase reactions with Cl atoms, OH radicals, and O_3, J. Photochem. Photobiol. A, 199, 92–97, https://doi.org/10.1016/j.jphotochem.2008.05.013, 2008.

Sulbaek Andersen, M. P., Nielsen, O. J., Karpichev, B., Wallington, T. J., and Sander, S. P.: Atmospheric chemistry of isoflurane, desflurane, and sevoflurane: Kinetics and mechanisms of reaction with chlorine atoms and OH radicals and global warming potentials, J. Phys. Chem., 116, 5806–5820, https://doi.org/10.1021/jp2077598, 2012.

Tewari, S. G., Vijayaraghavan, K., Zhao, K., David, L. M., Tuite, K., Kristanovich, F., Zhuang, Y., Yang, B., Hurtado, C., Papanastasiou, D. K., Giffen, P., Kimko, H., Gibbs, M., and Platz, S.: Atmospheric and watershed modelling of HFO-1234ze(E) emissions from prospective pressurized metered-dose inhalers usage, EGUsphere, in review, 2025, 1–21, https://doi.org/10.5194/egusphere-2025-1031, 2025.

Thacker, W. C.: Data assimilation with inequality constraints, Ocean Model., 16, 264–276, https://doi.org/10.1016/j.ocemod.2006.11.001, 2007.

Thomson, J. D., Campbell, J. S., Edwards, E. B., Medcraft, C., Nauta, K., Pérez-Peña, M. P., Fisher, J. A., Osborn, D. L., Kable, S. H., and Hansen, C. S.: Fluoroform (CHF_3) production from CF_3CHO photolysis and implications for the decomposition of hydrofluoroolefins and hydrochlorofluoroolefins in the atmosphere, J. Am. Chem. Soc., 147, 33–38, https://doi.org/10.1021/jacs.4c11776, pMID: 39714911, 2025.

United Nations: Montreal Protocol on Substances That Deplete the Ozone Layer. Montreal, 16 September 1987. Amendment to the Montreal Protocol on Substances That Deplete the Ozone Layer, Kigali, 15 October 2016, Tech. Rep. C.N.872.2016.TREATIES-XXVII.2.f (Depositary Notification), United Nations, New York, 10017, 2016.

US-AIM: Office of the Law Revision Counsel of the United States House of Representatives: AIR POLLUTION PREVENTION AND CONTROLSUBCHAPTER VII-AMERICAN INNOVATION AND MANUFACTURING, https://uscode.house.gov/view.xhtml?req=granuleid:USC-prelim-title42-section7675(a)&num=0&edition=prelim, last accessed 2025-02-24, 2020.

Van Hoomissen, D., Chattopadhyay, A., Montzka, S. A., and Burkholder, J. B.: CHF_3 (HFC-23) and CF_3CHO Quantum Yields in the Pulsed Laser Photolysis of CF_3CHO at 248, 266, 281, and 308 nm, ACS Earth Space Chem., 9, 589–602, https://doi.org/10.1021/acsearthspacechem.4c00316, 2025.

Vollmer, M. K., Miller, B. R., Rigby, M., Reimann, S., Mühle, J., Krummel, P. B., O'Doherty, S., J., K., Rhee, T. S., Weiss, R. F., Fraser, P. J., Simmonds, P. G., Salameh, P. K., Harth, C. M., Wang, R. H. J., Steele, L. P., Young, D., Lunder, C. R., Hermansen, O., Ivy, D., Arnold, T., Schmidbauer, N., Kim, K.-R., Greally, B. R., Hill, M., Leist, M., Wenger, A., and Prinn, R. G.: Atmospheric histories and global emissions of the anthropogenic hydrofluorocarbons HFC-365mfc, HFC-245fa, HFC-227ea, and HFC-236fa, J. Geophys. Res., 116, D08304, https://doi.org/10.1029/2010JD015309, 2011.

https://doi.org/10.5194/egusphere-2025-4824
Preprint. Discussion started: 7 October 2025

Vollmer, M. K., Reimann, S., Hill, M., and Brunner, D.: First observations of the fourth generation synthetic halocarbons HFC-1234yf, HFC-1234ze(E), and HCFC-1233zd(E) in the atmosphere, Environ. Sci. Technol., 49, 2703–2708, https://doi.org/10.1021/es505123x, 2015.

Vollmer, M. K., Young, D., Trudinger, C. M., Mühle, J., Henne, S., Rigby, M., Park, S., Li, S., Guillevic, M., Mitrevski, B., Harth, C. M., Miller, B. R., Reimann, S., Yao, B., Steele, L. P., Wyss, S. A., Lunder, C. R., Arduini, J., McCulloch, A., Wu, S., Rhee, T. S., Wang, R. H. J., Salameh, P. K., Hermansen, O., Hill, M., Langenfelds, R. L., Ivy, D., O'Doherty, S., Krummel, P. B., Maione, M., Etheridge, D. M., Zhou, L., Fraser, P. J., Prinn, R. G., Weiss, R. F., and Simmonds, P. G.: Atmospheric histories and emissions of chlorofluorocarbons CFC-13 ($CClF_3$), ΣCFC-114 ($C_2Cl_2F_4$), and CFC-115 (C_2ClF_5), Atmos. Chem. Phys., 18, 979–1002, https://doi.org/10.5194/acp-18-979-2018, 2018.

Western, L. M., Rigby, M., Mühle, J., Krummel, P. B., Lunder, C. R., O'Doherty, S., Reimann, S., Vollmer, M. K., Young, D., Adam, B., Fraser, P. J., Ganesan, A. L., Harth, C. M., Hermansen, O., Kim, J., Langenfelds, R. L., Loh, Z. M., Mitrevski, B., Pitt, J. R., Salameh, P. K., Schmidt, R., Stanley, K., Stavert, A. R., Wang, H.-J., Weiss, R. F., and Prinn, R. G.: Global Emissions and Abundances of Chemically and Radiatively Important Trace Gases from the AGAGE Network, Earth Syst. Sci. Data Disc., 2025, 1–41, https://doi.org/10.5194/essd-2025-348, 2025.